Available online at www.sciencedirect.com
ScienceDirect
Geochimica et Cosmochimica Acta 71 (2007) 3812–3832
Geochimica et Cosmochimica Acta
www.elsevier.com/locate/gca

Optically continuous silcrete quartz cements of the St. Peter Sandstone: High precision oxygen isotope analysis by ion microprobe

Jacque L. Kelly *, Bin Fu, Noriko T. Kita, John W. Valley

Department of Geology and Geophysics, University of Wisconsin, Madison, WI 53706, USA

Received 15 January 2007; accepted in revised form 15 May 2007; available online 2 June 2007

Abstract

A detailed oxygen isotope study of detrital quartz and authigenic quartz overgrowths from shallowly buried (<1 km) quartz arenites of the St. Peter Sandstone (in SW Wisconsin) constrains temperature and fluid sources during diagenesis. Quartz overgrowths are syntaxial (optically continuous) and show complex luminescent zonation by cathodoluminescence. Detrital quartz grains were separated from 53 rocks and analyzed for oxygen isotope ratio by laser fluorination, resulting in an average $\delta^{18}O$ of $10.0 \pm 0.2‰$ (1SD, $n = 109$). Twelve thin sections were analyzed by CAMECA-1280 ion microprobe (6–10 μm spot size, analytical precision better than ±0.2‰, 1SD). Detrital quartz grains have an average $\delta^{18}O$ of $10.0 \pm 1.4‰$ (1SD, $n = 91$) identical to the data obtained by laser fluorination. The ion microprobe data reveal true variability that is otherwise lost by homogenization of powdered samples necessary for laser fluorination. Laser fluorination uses samples that are one million times larger than the ion microprobe. Whole rock (WR) samples from the 53 rocks were analyzed by laser fluorination, giving $\delta^{18}O$ between 9.8‰ and 16.7‰ ($n = 110$). Quartz overgrowths in thin sections from 10 rocks were analyzed by ion microprobe and average $\delta^{18}O = 29.3 \pm 1.0‰$ (1SD, $n = 161$).

Given the similarity, on average, of $\delta^{18}O$ for all detrital quartz grains and for all quartz overgrowths, samples with higher $\delta^{18}O$(WR) values can be shown to have more cement. The quartz cement in the 53 rocks, calculated by mass balance, varies from <1 to 21 vol.% cement, with one outlier at 33 vol.% cement. Eolian samples have an average of 11% cement compared to marine samples, which average 4% cement.

Two models for quartz cementation have been investigated: high temperature (50–110 °C) formation from ore-forming brines related to Mississippi Valley Type (MVT) mineralization and formation as silcretes at low temperature (10–30 °C). The homogeneity of $\delta^{18}O$ for quartz overgrowths determined by ion microprobe rules out a systematic regional variation of temperature as predicted for MVT brines and there are no other known heating events in these sediments that were never buried to depths >1 km. The data in this study suggest that quartz overgrowths formed as silcretes in the St. Peter Sandstone from meteoric water with $\delta^{18}O$ values of −10‰ to −5‰ at 10–30 °C. This interpretation runs counter to conventional wisdom based on fibrous or opaline silica cements suggesting that the formation of syntaxial quartz overgrowths requires higher temperatures. While metastable silica cements commonly form at high degrees of silica oversaturation following rapid break-down reactions of materials such as of feldspars or glass, the weathering of a clean quartz arenite is slower facilitating chemical equilibrium and precipitation of crystallographically oriented overgrowths of α-quartz.

* Corresponding author.
E-mail address: jacquelkelly@yahoo.com (J.L. Kelly).

0016-7037/$ - see front matter © 2007 Elsevier Ltd. All rights reserved.
doi:10.1016/j.gca.2007.05.014

1. INTRODUCTION

The compositions and temperatures of fluids that have passed through quartz arenite sandstones are enigmatic because little evidence of their passage remains. Oxygen isotopes from syntaxial quartz overgrowths in clean quartz-rich sandstones, like the St. Peter Sandstone, may provide the best record of paleofluid compositions, temperatures, and histories of diagenetic fluid–rock interaction. These data preserve information regarding different processes responsible for quartz overgrowth formation, which may have taken place at various times throughout the burial history of the St. Peter Sandstone.

Oxygen isotope analysis by laser fluorination can reveal intra-and inter-sample variation in $\delta^{18}O$ of detrital quartz (DQ), quartz overgrowths (cement), and whole rock samples (WR = detrital quartz plus quartz overgrowths). Laser fluorination is a useful compliment to in situ analysis, especially given its high analytical accuracy and precision (0.07‰, 1SD; Valley et al., 1995; Spicuzza et al., 1998), however; this method requires 1–2 mg of sample per analysis (100–150 grains of quartz at 150–300 μm diameter). Thus, laser fluorination cannot measure single detrital grains or fine-scale (10–20 μm) zoning of $\delta^{18}O$ within the 10–100 μm overgrowths, which has been reported in the St. Peter Sandstone (Graham et al., 1996).

Estimation of the volume percent of quartz cement from $\delta^{18}O$(WR) and $\delta^{18}O$(DQ) values attained by laser fluorination is possible if the $\delta^{18}O$(cement) values are known and have a limited range in value. The values of $\delta^{18}O$ for detrital quartz and quartz cement have been estimated using laser fluorination data after samples were prepared by a technique developed by Lee and Savin (1985) that isolates overgrowths from detrital quartz grains. However, such bulk analyses are generally of mixtures and give inaccurate results (Graham et al., 1996). A better method for determining $\delta^{18}O$(cement) is through in situ analysis by ion microprobe.

Oxygen isotope analysis by ion microprobe is a high spatial resolution (1–10 μm) method of in situ measurement that analyzes a sample volume one million times smaller than laser fluorination methods. The analytical precision of this study is 0.1‰ to 0.2‰ (1SD). Thus, the ion microprobe can analyze oxygen isotope ratios at the fine scale necessary to decipher the formation history of these quartz cements. The ion microprobe can also investigate possible oxygen isotope heterogeneity associated with different stages of overgrowth development recognized in several studies of the St. Peter Sandstone (Pittman, 1972; Odom et al., 1979; Pitman et al., 1997).

This study will use in situ oxygen isotope analysis of authigenic quartz overgrowths to investigate the compositions, temperatures, and fluid–rock interaction history of fluids responsible for quartz cementation in the shallowly buried (<1 km) St. Peter Sandstone on the Wisconsin Dome. It does not investigate quartz cements of the more deeply buried (>2.5 km) sandstone in the Michigan and Illinois Basins (Hoholick et al., 1984; Graham et al., 1996; Pitman et al., 1997). These oxygen isotope data will be used to test two competing models in which quartz cement either formed at higher temperatures (50–110 °C) from hydrothermal ore-forming brines related to Mississippi Valley Type (MVT) mineralization in SW Wisconsin or at low temperatures (10–30 °C) in a near surface environment as silcretes. Habermann (1978) reports silcrete cements immediately below erosional surfaces at the top of some St. Peter Sandstone outcrops and Smith et al. (1997) report microcrystalline silica immediately below a major unconformity directly beneath the St. Peter Sandstone. This study investigates regionally distributed samples with no apparent relation to erosion surfaces. The St. Peter Sandstone is ideal for this application given its wide-spread distribution and its content of ubiquitous, though sparse quartz overgrowths.

2. GEOLOGIC BACKGROUND

2.1. Regional geology

The Middle Ordovician St. Peter Sandstone is a super mature quartz arenite consisting of ~97% quartz and characterized by well-rounded monocrystalline quartz sand grains (Odom et al., 1979; Mai and Dott, 1985; Pitman et al., 1997; Kelly, 2006). The sandstone is a spatially extensive (~600,000 km^2), laterally continuous sheet of clastic sediments in areas of Wisconsin, Minnesota, Illinois, Michigan, Iowa, Missouri, and Arkansas (Dapples, 1955; Mai and Dott, 1985; Shepherd et al., 1994). The sandstone's composition, permeability, and distribution make it a regional aquifer (Mai and Dott, 1985; Pitman et al., 1997).

Maximum burial depths of the St. Peter Sandstone vary. Present day burial exceeds 2.5 km in the Michigan and Illinois Basins; however, in southwestern Wisconsin, the St. Peter Sandstone is exposed on the Wisconsin Dome and several lines of evidence indicate that it has never been buried deeply. Cambrian through Devonian strata thin significantly moving from the basins onto the dome indicating that the area of SW Wisconsin has been part of a dome since deposition of the St. Peter Sandstone. Regional stratigraphy in southern Wisconsin indicates that Silurian, Devonian, and possibly minor Mississippian marine units extended across this area and their combined thicknesses, where preserved, are less than 500 m. Since the Mississippian, Wisconsin has been above sea level and has not been receiving sediments. Thus, a maximum burial depth of 1 km is conservative and may slightly overestimate depths (Hoholick et al., 1984; Mai and Dott, 1985; Rowan and Goldhaber, 1996; Pitman et al., 1997; Prothero and Dott, 2004).

An interregional unconformity (Fig. 1), which designates the disconformable base of the St. Peter Sandstone, formed during an erosional episode of considerable duration (perhaps tens of millions of years), during which well-established drainage patterns (Figs. 1 and 2) and karst topography (Fig. 2) developed. Variation and local thickening from 0–120 m in Wisconsin and Illinois occurs and has been attributed to the highly irregular pre-St. Peter Sandstone erosional surface (isopachs in Fig. 2; Sloss, 1963; Mai and Dott, 1985).

The St. Peter Sandstone contains three units, the Readstown, Tonti, and Glenwood Members (Fig. 1). This study focuses on the Tonti Member. This member is composed of two lithofacies, the large-scale cross bedded lithofacies (eolian) and the medium-scale cross bedded and burrowed lithofacies (marine; Winfree, 1983). For brevity in the rest

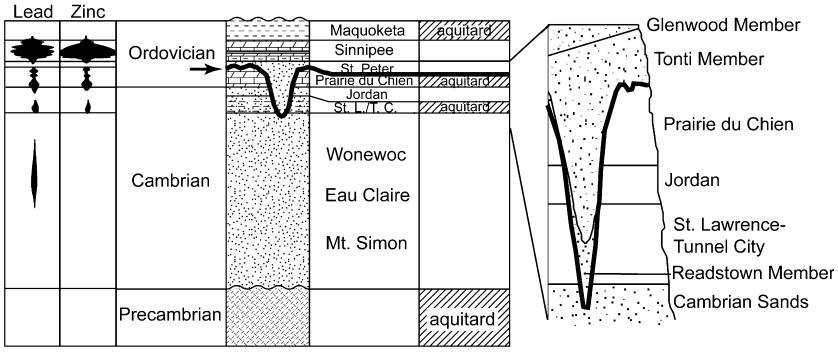

Fig. 1. Stratigraphic cross-section of the Cambrian and Ordovician sediments of SW Wisconsin. The arrow and bold line mark the sub-St. Peter Sandstone unconformity. "St. L." represents the St. Lawrence group and "T.C." represents the Tunnel City Formation. The vertical channel depicts a paleo-river valley later filled in by the St. Peter Sandstone (after Heyl et al., 1959; Ostrom, 1967; Arnold et al., 1996).

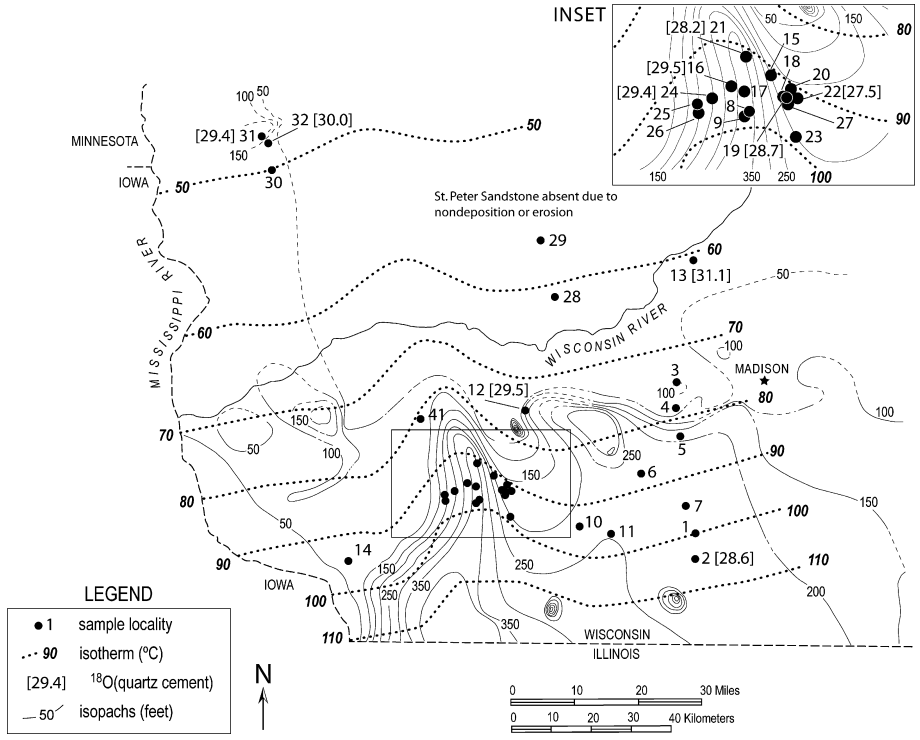

Fig. 2. Pre-St. Peter Sandstone erosional surface (isopachs contoured in feet) of SW Wisconsin (Mai and Dott, 1985). The isotherms of Arnold et al. (1996) are shown in (°C). All samples except one were collected from Tonti Member outcrops. All samples are designated by locality (given in Table 1). Minnesota samples (localities 33–40) are from near Faribault and Minneapolis/St. Paul. The average $\delta^{18}O$(cement) value relative to V-SMOW for each of the 10 samples analyzed by ion microprobe is given in brackets. Further description of sample locations is given in Kelly (2006). Two sharply contoured oval isopachs represent karst features and one set of concentric isopachs is a paleo-hill. A north to south paleo-river valley exists in the central part of the study area most of which is shown in the inset.

of the paper the interpretative terms eolian and marine will be used. After deposition of the St. Peter Sandstone and following an interval of non-deposition, Sinnipee Group carbonates formed as a transgression flooded the craton from the southeast (Mai and Dott, 1985).

2.2. Diagenesis and petrography

The St. Peter Sandstone in SW Wisconsin has experienced a complex diagenetic history (Mai and Dott, 1985). In the shallowly buried sandstone, primary porosity predominates (up to 30%) and there is only minor secondary dissolution of cements (Odom et al., 1979; Hoholick et al., 1984). Minor pressure solution has been documented, but is not sufficient to be the dominant source of silica responsible for overgrowth formation (Odom et al., 1979; Kelly, 2006). Conversely, where the St. Peter Sandstone is deeply buried (>2.5 km) in the Michigan and Illinois Basins, a series of diagenetic events have modified the sandstone's texture, porosity, and permeability (Hoholick et al., 1984; Drzewiecki et al., 1994; Pitman et al., 1997).

Petrographic microscope investigation in plain and cross-polarized transmitted light shows that optically continuous quartz overgrowths are the dominant diagenetic mineral in the shallowly buried St. Peter Sandstone. No fluid inclusions were seen within the quartz overgrowths. "Dust rims" occur on many detrital quartz grains at the boundary with overgrowths in several, but not all samples. Minor late calcite was identified in a few samples after staining with alizarin red. No opal, fibrous silica cements, pyrite, or kaolinite were observed in thin section.

Quartz overgrowths are syntaxial cements (optically continuous with detrital quartz grains). The overgrowths formed early in the history of the St. Peter Sandstone (Odom et al., 1979; Hoholick et al., 1984). Quartz overgrowths occur on most grain surfaces in all samples, consistent with observations by Odom et al. (1979). Two samples (05-WI-29 and 05-WI-36) show voids and cracks due to quartz dissolution. The overgrowths in these samples are partially detached from and not optically continuous with their corresponding detrital quartz grains.

Quartz overgrowths develop in a series of stages as observed by Waugh (1970) for northern England Penrith Sandstone samples and by Pittman (1972) for St. Peter Sandstone samples. First, the growth of optically continuous projections of quartz on grain surfaces begins. Continued growth results in larger faces with recognizable prismatic or rhombohedral form. A final growth stage produces polyhedral quartz crystals (Waugh, 1970). In this respect, adjacent growth projections can coalesce and form one coherent quartz overgrowth around a single detrital quartz grain (Austin, 1974; Odom et al., 1979).

Recrystallization of fibrous silica cements (opal and chalcedony) to syntaxial quartz is documented in some terranes, but is rare at low temperatures (Summerfield, 1983a). When recrystallization does occur, an isopachous ghost may be present, which suggests an amorphous precursor. Goldstein and Rossi (2002) propose that it takes temperatures over 180 °C to recrystallize fibrous quartz. None of the textural features or styles indicating recrystallization have been observed in the samples of this study, including preservation of primary growth features (i.e. fine growth banding), preferential replacement, and crosscutting relationships (i.e. irregular and scalloped margins). Thus, there is no evidence of recrystallization in the cements of this study.

2.3. Previous research

Graham et al. (1996) initially determined oxygen isotope ratios ($\delta^{18}O$) of St. Peter Sandstone samples from the Wisconsin Dome and the Michigan Basin by externally heated Ni-reaction vessels and by laser fluorination. Samples were lightly crushed, treated with hydrofluoric acid, and ultrasonically disaggregated. Detrital quartz grains were lightly crushed and visible quartz overgrowth was removed by air abrasion for two samples. After sieving, it was found that the finest sieve fractions were higher in $\delta^{18}O$ than the coarsest sieve fractions by 5–12‰ for Wisconsin Dome samples and by 2–5‰ for samples from the Michigan Basin. This correlation supported the hypothesis that overgrowths were concentrated in the finest sieve fractions and detrital quartz in the coarsest sieve fractions, and that overgrowths formed at higher temperatures in the deeply buried samples from the Michigan Basin. This method suggested that the $\delta^{18}O$ of quartz cement is between 16.8‰ and 26.8‰ for Wisconsin Dome samples and between 12.6‰ and 16.0‰ for Michigan Basin samples. Coarse sieve fractions inferred to be detrital quartz typically give $\delta^{18}O$ from 10–12‰ regardless of the sample's geographic location or depth of burial (Graham et al., 1996).

Four samples of St. Peter Sandstone were also analyzed for $\delta^{18}O$ by a single collector CAMECA ims-4f ion microprobe at the University of Edinburgh by Graham et al. (1996). These analyses show that $\delta^{18}O$(DQ) averages 9.2 ± 2.0‰ (1SD, $n = 25$) for two Wisconsin Dome samples and 9.4 ± 1.6‰ (1SD, $n = 46$) for two Michigan Basin samples. Furthermore, $\delta^{18}O$(cement) for the Wisconsin Dome samples averages 25.4 ± 3.8‰ (1SD, $n = 25$), while Michigan Basin samples average 16.1 ± 2.5‰ (1SD, $n = 36$).

Graham et al. (1996) concluded that quartz overgrowths from the Michigan Basin formed from basin brines or formation waters at high temperatures between 135 and 205 °C, with little or no meteoric water component. These formation temperatures reflect the lower $\delta^{18}O$(cement) values found in the Michigan Basin samples.

Graham et al. (1996) suggested two models for quartz cementation on the Wisconsin Dome. One model hypothesized cementation at ambient burial temperatures with little or no regional fluid flow. This model predicted quartz overgrowth formation from a fluid dominated by low $\delta^{18}O$ meteoric water at temperatures less than 50 °C. The second model hypothesized coeval quartz cementation with heated basin brines that are known to have been responsible for Mississippi Valley Type ore mineralization in the Upper Mississippi Valley lead–zinc district. This hypothesis was based on the basin brine fluid flow model of Arnold et al. (1996), which predicts systematic temperature variations as northward migrating fluids cool from 110–50 °C throughout southwestern Wisconsin (isotherms in Fig. 2; Graham et al., 1996).

2.4. Mississippi Valley Type (MVT) mineralization

Timing of events is critical to evaluate the possible linkage of quartz overgrowth formation to MVT mineralization. The Upper Mississippi Valley (UMV) lead–zinc district formed at 270 ± 4 Ma (Permian) when hydrothermal brines precipitated galena and sphalerite primarily in Sinnipee Group carbonates, which overly the St. Peter Sandstone (Fig. 1; Mai and Dott, 1985; Bethke, 1986; Brannon et al., 1992). Brine migration was likely caused by uplift near the southern end of the Illinois Basin in response to the Ouachita Orogeny (Bethke, 1986; Garven et al., 1993; Rowan and Goldhaber, 1996) and tectonically-controlled, gravity-driven brine flow out of the Illinois Basin and onto the Wisconsin Dome (Garven and Freeze, 1984a,b; Garven et al., 1993; Pitman and Spotl, 1996; Rowan and Goldhaber, 1996; Pitman et al., 1997). The St. Peter and underlying sandstones acted as aquifers, carrying these heated migrating brines (Pitman et al., 1997). In SW Wisconsin, it is hypothesized that basin brines that were confined in sand-

stone aquifers escaped upwards through the permeable St. Peter Sandstone where it filled paleo-river valleys that locally removed the previously underlying fine-grained sediments of the Prairie du Chien, St. Lawrence, and Tunnel City units, that otherwise acted as aquitards (Fig. 1). This breaching mechanism may be responsible for localized mineralization, especially in the central portion of the study area where a north to south paleo-river valley exists beneath a concentration of lead and zinc deposits (Fig. 2; Mai and Dott, 1985; Arnold et al., 1996; Rowan and Goldhaber, 1996).

Understanding the thermal history of migrating brines that flowed throughout SW Wisconsin will provide a strong foundation for evaluating whether quartz overgrowths formed from these brines. Arnold et al. (1996) used numerical modeling at two scales to determine that brines cooled as they flowed northward through the UMV district. Modeling at the individual ore body scale was done through characterization of fracture patterns in Sinnipee group carbonate host strata by two-dimensional flow in discrete fracture networks. Larger-scale processes of groundwater flow and heat transport were investigated using three-dimensional models. This approach gives regional temperatures between 50 and 110 °C at the top of the St. Peter Sandstone (isotherms in Fig. 2) assuming 10 m/yr discharge of hydrothermal fluids from the Illinois Basin. These results are in good agreement with sphalerite fluid inclusion data from the UMV district (Bailey and Cameron, 1951; McLimans, 1977), quartz fluid inclusion studies by Pitman et al. (1997) in the Illinois Basin, as well as a model by Bethke (1986). Thus, if quartz cementation was coeval with hydrothermal brine migration, then quartz overgrowths should record formation temperatures near 110 °C along the Illinois border that systematically decrease to near 50 °C at the northern end of the study area.

Sverjensky (1981) used $\delta^{18}O$ and $\delta^{13}C$ isotopic measurements of host rock limestone, dolostone, and gangue calcite from the UMV district to model open and closed system exchange of carbon and oxygen isotopic compositions of calcite as a function of water to rock ratio. The results of this study show that the water responsible for isotopic alteration of the carbonate host rocks ranges in $\delta^{18}O$ from +2‰ to +3‰ at 100 °C.

2.5. Silcrete formation

In contrast to the MVT model, if quartz cementation in the St. Peter Sandstone occurred before burial, the process may represent the formation of a siliceous duricrust or silcrete. Silcretes are typically classified into two categories, those forming within a few meters of the Earth's surface, and those forming more deeply, near the groundwater table (Watts, 1978; Thiry and Milnes, 1991; Thiry and Simon-Coincon, 1996; Webb and Golding, 1998; Alexandre et al., 2004). Silcretes are most commonly reported in rocks from areas where silcrete formation is still ongoing and thus, many older silcretes may be unrecognized. This view is also discussed by Summerfield (1983a).

Several factors govern silica deposition at near surface temperatures. These factors include whole rock composition, chemical reactions, prolonged subaerial exposure, relatively slow rates of tectonic uplift and erosion, long term stability of the sediment surface, water chemistry fluctuations, and high evaporation rates (Folk and Pittman, 1971; Smale, 1973; Summerfield, 1983a; Summerfield, 1983b; Murray, 1990; Thiry and Milnes, 1991; Rodas et al., 1994; Smith et al., 1997; Webb and Golding, 1998; Alexandre et al., 2004).

The textural, mineralogical, and oxygen isotope characteristics of a silcrete are principally determined by the host rock, the geochemical environment during cementation, and any recrystallization or replacement that has taken place. The lithology of the host rock in which a silcrete forms may be the most important factor controlling silica deposition (Smale, 1973; Summerfield, 1983a; Khalaf, 1988; Murray, 1990). For example, Smale (1973) attributes the formation of syntaxial overgrowths as the response of quartz arenites to the silcrete-forming process. Such silcretes are petrographically identical to sedimentary orthoquartzites. Thus, in these studies, the main factor used to distinguish silcretes from orthoquartzites is the observation that they are actively forming on the surface today, but geochemical tests were not applied.

The $\delta^{18}O$ of silcrete forming fluids is controlled by the composition of local meteoric water and any processes that may modify it. During deposition of the St. Peter Sandstone, Wisconsin was located near the equator (McElhinny, 1973; McElhinny and Opdyke, 1973). After deposition of the sandstone, the study area moved to its current position of 40°N. Since the $\delta^{18}O$ values of meteoric water vary with latitude, meteoric water responsible for overgrowth formation between the equator and 40°N would range from nearly −12‰ to −3‰ (closer to −3 for the equator; IAEA, 1981) However, for both the high and low temperature models considered here, overgrowth formation was early in the St. Peter Sandstone's history; thus, meteoric water responsible for overgrowth formation was likely closer to −3‰, reflecting deposition closer to equatorial latitudes. This $\delta^{18}O$ value is 5–6‰ lower than the composition of MVT ore-forming brines estimated by Sverjensky (1991).

3. METHODS

3.1. Sample collection

Samples were collected from outcrops in SW Wisconsin and SE Minnesota (Fig. 2; Kelly, 2006). All samples but one were collected from the Tonti Member of the St. Peter Sandstone, as this unit is composed predominantly of quartz (~97%). Physically resistant samples from each outcrop were sought based on the assumption that these samples contain more quartz cement. Areas with visible iron cement were avoided. Detailed sampling was conducted to investigate the possible correlation of overgrowths and basin brine fluids channeling through a paleo-river valley in the central portion of the study area near abandoned galena and zinc mines around Mineral Point, Wisconsin (Figs. 1 and 2). This paleo-river valley may have focused basin brines concentrating Mississippi Valley Type lead and zinc mineralization in Sinnipee Group carbonates directly above the breached aqui-

tards (Mai and Dott, 1985; Arnold et al., 1996; Rowan and Goldhaber, 1996).

3.2. Cathodoluminescence

Cathodoluminescence (CL) images of detrital quartz grains and their corresponding authigenic quartz overgrowths were collected using a Centarus Detector on a JEOL JSM-6360LV Scanning Electron Microscope (SEM) at Colgate University, with an accelerating voltage of 15 kV. After image collection, brightness and contrast were modified with Adobe Photoshop to articulate finer features in the quartz overgrowths and detrital quartz grains. Secondary electron (SE) images corresponding to the exact area of each CL image were collected for reference and used for targeting ion microprobe analysis pits.

Cathodoluminescence and SE images were also taken with a Gatan PanaCL/F imaging system on a Hitatchi S-3400 N SEM at the University of Wisconsin, Madison using an accelerating voltage of 15 kV. This system is equipped with a parabolic mirror and photomultiplier tube, which detects luminescence from UV to near-IR (185–850 nm). This second set of images was collected after ion microprobe analysis. These images record ion microprobe pits and aid in identification of the type of material analyzed by ion microprobe; for instance whether the pits sampled detrital quartz, quartz overgrowths, or mixtures of these two components. Grain images of the St. Peter Sandstone were also taken with the Hitatchi S-3400 N SEM using an accelerating voltage of 15 kV.

3.3. Oxygen isotope analysis

3.3.1. Sample preparation for laser fluorination analysis

St. Peter Sandstone samples were prepared to concentrate quartz in three fractions for oxygen isotope analysis by laser fluorination: whole rock (WR), whole quartz grains (WQG), and detrital quartz (DQ, Electronic annex EA-1). The WR and WQG samples contain detrital quartz and quartz overgrowths, while the DQ samples are virtually overgrowth free. The preparation for each of these fractions is described below and further explanation is given by Kelly (2006).

Whole rock samples from 19 rocks were prepared by disaggregating approximately half a gram of material from a small area in each rock. The collected sandstone was lightly ground by mortar and pestle to detach grains from each other and then treated with 37.4 wt% HCl at room temperature for 24 h to remove traces of carbonate. The sample was then powdered by mortar and pestle (EA-1).

Preparation of whole quartz grains (WQG, 150–300 μm diameter grains) began by disaggregating about five grams of sand from each of 53 rocks. This material was lightly ground by mortar and pestle to detach grains from each other and then treated with 37.4 wt% HCl at room temperature for 24 h to remove carbonates. Each sample was then sieved generating a fraction of 150–300 μm diameter grains (EA-1). Thirty out of 53 samples have more than 50 wt% of their grains in the 150–300 μm fraction, while sixteen samples have a majority of grains coarser than 300 μm and four samples have a majority of grains finer than 150 μm. Three samples have between 46 and 48 wt% of their grains in the 150–300 μm fraction, which still constitutes the majority of the grains in the sample, when compared to the other sieve fractions (Kelly, 2006). At least 0.5 g of the 150–300 μm fraction was saved for WQG analysis.

A portion of the unsieved WQG sample was used to generate each detrital quartz sample. Fifty milliliters of 49 wt% HF at room temperature was used to treat each gram of WQG sample for 60–150 min to dissolve quartz cement. Each sample was then sieved to separate 150–300 μm diameter detrital quartz grains (EA-1). Each WQG sample was weighed before HF treatment and the resulting detrital quartz sample was weighed after HF treatment to determine the amount of quartz loss, which ranges between 20 and 70 wt%. Since the maximum volume percent of quartz cement is 21% (excluding one outlier at 35%), this sample preparation procedure removed all quartz cement, a result confirmed by inspection of the grains after treatment with a binocular microscope.

3.3.2. Analysis by laser fluorination

Oxygen isotope analyses of silicates were conducted in the Stable Isotope Laboratory at the University of Wisconsin, Madison. All data are reported in standard per mil (‰) notation relative to V-SMOW. The fractionation of oxygen isotopes between quartz and water, $\Delta^{18}O(Qtz\text{-}H_2O)$, is calculated from the lower temperature (200–500 °C) equation and 1 kb experiments by Clayton et al. (1972), which are in good general agreement with the 15 kb experiments of Hu and Clayton (2003). Extrapolation of these results to 10 °C yields good agreement with empirical estimates based on diatoms (Labeyrie, 1974).

Oxygen was liberated from samples by heating in an atmosphere of BrF_5 using a CO_2 laser. Oxygen was cryogenically purified and converted to CO_2 for analysis with a Finnigan MAT 251 mass spectrometer (Valley et al., 1995; Spicuzza et al., 1998). All analyses are standardized using the Gore Mountain Garnet standard (UWG-2) and the accepted $\delta^{18}O$ value of 5.8‰ (Valley et al., 1995). The average $\delta^{18}O$(raw) value of UWG-2 for 16 analysis days was 5.70 ± 0.09‰ (1SD, $n = 100$). Twelve analyses of NBS-28 quartz on four separate days give an average $\delta^{18}O$ of 9.46 ± 0.06‰ V-SMOW (1SD).

3.3.3. Sample preparation for ion microprobe analysis

Twelve thin sections were embedded with one grain of the University of Wisconsin quartz standard (UWQ-1), which was analyzed by laser fluorination and has a $\delta^{18}O$ value of 12.33 ± 0.07‰ (1SD, $n = 29$; $1SE = \pm 0.01$‰; Kelly, 2006). Ten thin sections have standard grains mounted within 5 mm of the center of a "one-inch round" (25.4 mm) thin section, while two thin sections have standard grains mounted 5–9 mm from the center of the round thin section. All standard quartz grains and samples were polished together by diamond followed by colloidal silica for a smooth, flat, low-relief surface. Samples were then gold-coated in preparation for ion microprobe analysis.

3.3.4. Analysis by ion microprobe

Oxygen isotope ratios of detrital quartz and authigenic quartz overgrowths were measured for twelve rocks using a CAMECA ims-1280 ion microprobe. These analyses were conducted at Wisc-SIMS, the Wisconsin Secondary Ion Mass Spectrometer Laboratory at the University of Wisconsin, Madison.

The ~3 nA $^{133}Cs^{+}$ primary ion beam (20 keV total accelerating voltage) was focused to a diameter of 6–10 μm on the sample surface, and the secondary O^{-} ions were accelerated by −10 kV. An electron flood gun was used for charge compensation. The secondary ion optics are similar to those described in Kita et al. (2004, 2007), which aim to achieve high secondary ion transmission. Details of alignment include: transfer lens magnification of 200, contrast aperture (CA) 400 μm diameter, field aperture (FA) 4000 by 4000 μm square, entrance slit 122 μm wide, energy slit 40 eV wide, and exit slit 500 μm wide. Under these conditions, secondary ions from the analysis spot are almost fully transmitted through the CA, FA, and entrance slit. The intensity of ^{16}O was typically 2.5×10^{9} counts per second. The mass resolving power was about 2500, enough to remove hydride interferences on ^{18}O. Two faraday cups were used to measure ^{16}O and ^{18}O simultaneously, equipped with different resistors (10^{10} and 10^{11} Ω, respectively). The baseline of the Faraday cup detectors was measured once each day; drift during the day was insignificant compared to the noise level of the detectors (⩽1000 counts per second for the 10^{11} Ω resistor). Before each isotopic measurement, any small misalignment of the secondary optics (X, Y) was automatically tuned by a computer scan of the deflectors, while Z was manually adjusted if necessary. Total analytical time per spot was about 5 min, including locating and selecting the analytical positions, pre-sputtering (10 s), automatic retuning of the secondary ions (~60 s), and integration of the oxygen isotope signals (80 s).

Ion microprobe analyses of 10 samples were made in one 42 h period on December 21–22, 2005. Two additional samples were analyzed on May 12, 2006. At least eight standard analyses including a minimum of four analyses before and after each group of 7–19 sample analyses were used to correct the data shown in Electronic Annex EA-2. The average of these bracketing standard analyses determined the instrumental mass fractionation based on the accepted UWQ-1 value of 12.33‰. The values of instrument bias for quartz varied from −3.34‰ to −5.17‰ in December and from −5.35‰ to −5.72‰ in May.

3.4. X-ray fluorescence (XRF) analysis

At least 2.5 g of whole rock from 23 samples were disaggregated and powdered by mortar and pestle (EA-1). These samples were sent to SGS Laboratories in Toronto, Ontario, Canada for XRF analysis to determine the concentrations of the following eleven elements by a fused disk method, expressed as oxides: SiO_2, Al_2O_3, CaO, MgO, Na_2O, K_2O, Fe_2O_3, MnO, TiO_2, P_2O_5, and Cr_2O_3.

4. RESULTS

4.1. Quartz imaging

The SEM image of lightly crushed quartz grains (Fig. 3) shows the terminated nature of quartz overgrowths in the St. Peter Sandstone. Interlocking overgrowths are fairly common (Fig. 3). The overgrowths in this image hint at their complexity, which can be more fully seen through cathodoluminescence (CL) images of the polished grains

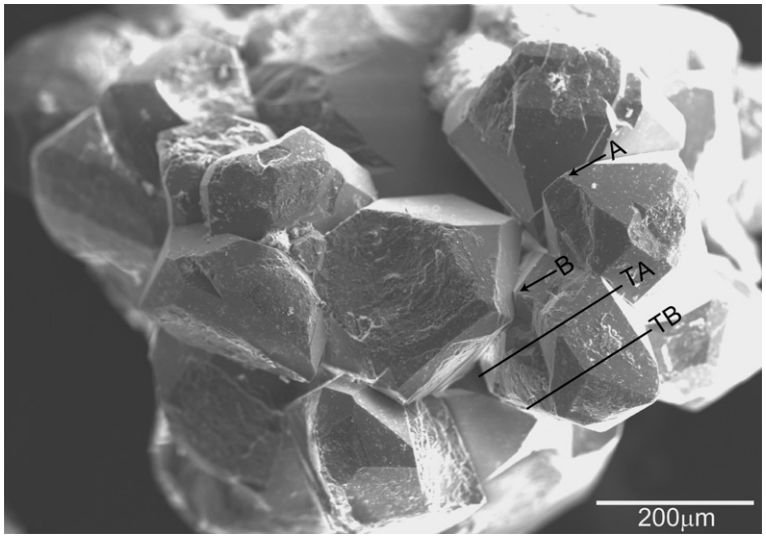

Fig. 3. Grain image of sample 04-WI-21 from the St. Peter Sandstone in SW Wisconsin. "A" points to an example of typical quartz overgrowth terminations seen in the samples of this study. "B" points to an example of interlocking overgrowths. The transects "TA" and "TB" demonstrate how one quartz grain cut in two different places for thin section preparation will result in different overgrowth textures. The transect "TA" will show a quartz overgrowth similar to the right side of the largest grain in Fig. 4a (labeled TA) while the transect "TB" will show a quartz overgrowth similar to the top left grain in Fig. 4a (labeled TB).

(Fig. 4a, c, and e). Cathodoluminescence shows that a variety of overgrowth shapes and textures are manifested in the shallowly buried St. Peter Sandstone (Fig. 4a, c, and e). These overgrowths appear to all relate to a single continuum process, which can be understood by comparing the grain image (Fig. 3) to the CL images (Fig. 4a, c, and e). Visualizing the three-dimensional relationships of the overgrowths and relating them to the two-dimensional thin-section view shows how different types of overgrowth shapes form. For instance, if a transect is cut across a grain (TA in Fig. 3), the result will be similar to the texture observed on the right side of the largest grain in Fig. 4a labeled "TA". Furthermore, if a transect is cut across the same grain (TB in Fig. 3), but in a different position, the result will be roughly approximate to the texture observed on the top left grain in Fig. 4a labeled "TB".

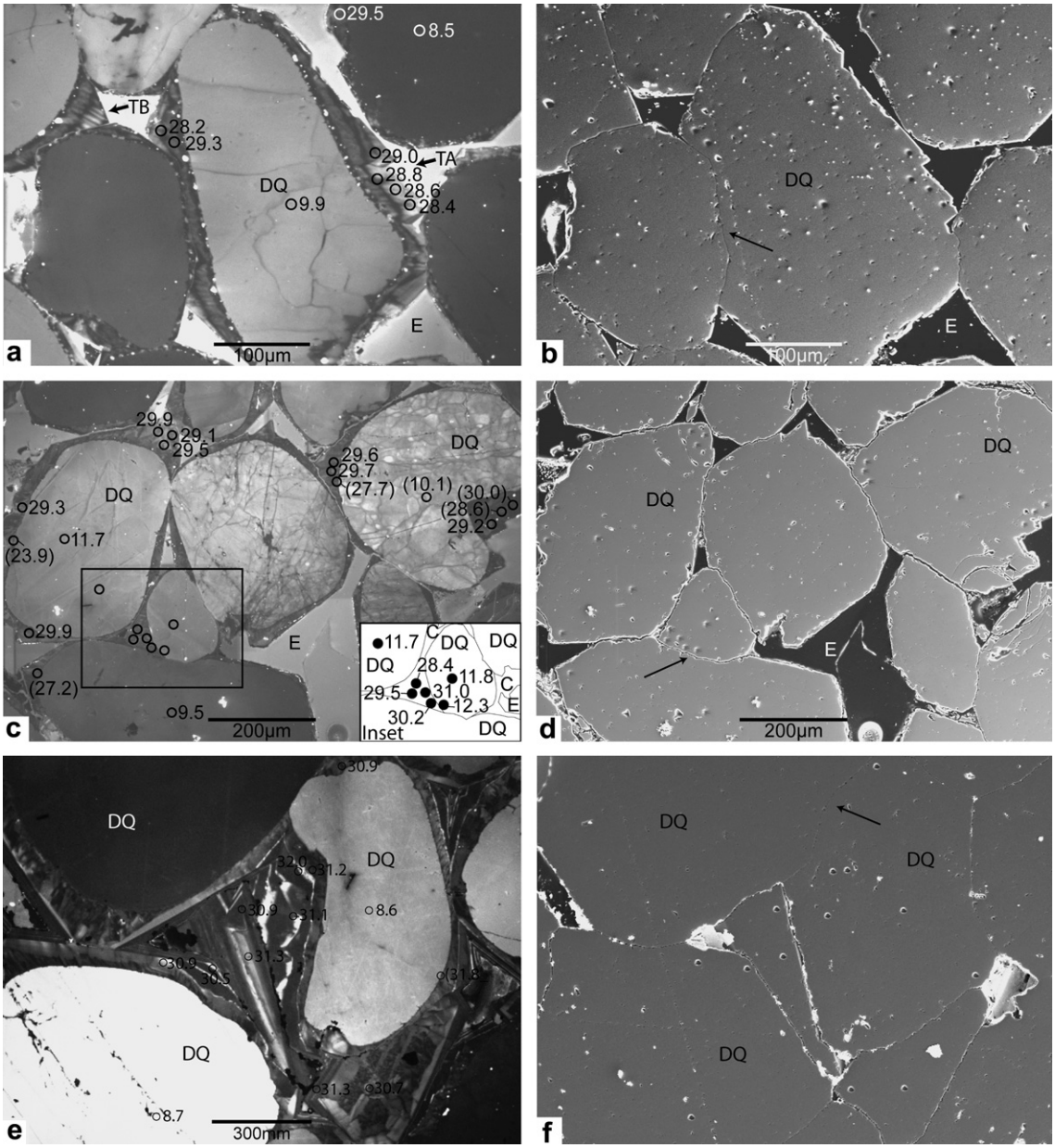

Fig. 4. Cathodoluminescence (CL, left) and corresponding secondary electron (SE, right) images. Ion microprobe analysis pits are shown as circles in CL and as depressions in SE. In all images DQ, detrital quartz; E, epoxy and C, quartz cement. All oxygen isotope ratios for ion microprobe pits are shown. Mixed analyses or analyses on cracks are given in parentheses. (a and b) Sample 04-WI-04-2 showing perpendicular finer features within the overgrowth in the top left corner. Note the dark to light cement pattern on the largest grain in this image as well as the similar orientation and shape of "outer" overgrowths and the overgrowth closest to the detrital quartz grain. "TA" and "TB" refer to the transects discussed in Fig. 3 and in the text. An arrow points to an overgrowth growing adjacent to and around a nearby detrital quartz grain in (b). (c and d) Sample 04-WI-21-2 showing complex zonation within the overgrowth. An arrow points to a point of detrital grain contact with minor pressure solution in (d). (e and f) Sample 04-WI-17B showing extremely complex quartz overgrowth textures. Pore space has been almost completely occluded by overgrowth formation as seen in (f). An arrow points to pressure solution in (f).

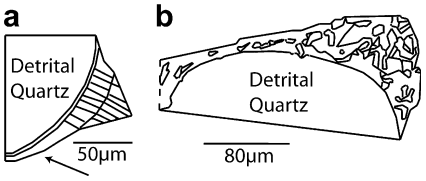

Fig. 5. Digitized images of quartz overgrowths in the St. Peter Sandstone from SW Wisconsin as shown by CL. (a) Detrital quartz grain in sample 04-WI-04-2 and overgrowth from the top left corner of Fig. 4a. Overgrowth image shows textures perpendicular to the main direction of overgrowth formation. An arrow points to the position of an adjacent detrital quartz grain not digitized in this image. (b) Grain and overgrowth digitized from the grain positioned in the center left of Fig. 4c from sample 04-WI-21-2. The overgrowth has complex luminescent zonation and continues beyond the dashed line on the left side of the figure.

Weak luminescence is common to the overgrowths in this study. This causes the overgrowth to be dark compared to detrital quartz grains when viewed by CL (Sippel, 1969; Sprunt and Nur, 1981). Additionally, several thin sections have overgrowths with a gradational change from weak luminescent areas closest to detrital quartz grains to brighter luminescent areas further from the quartz grains (Fig. 4a, c, and e) giving the appearance of multiple overgrowths. Furthermore, the growth of brighter CL areas usually mimics the overgrowth shape of darker areas (Fig. 4a, c, and e). This process may be related to overgrowths growing in stages, indicating changes in the formation conditions. Multiple quartz overgrowths were also observed by Austin (1974) for samples from the Shakopee Formation in Minnesota.

Two varieties of fine structure within these overgrowths are visible in CL. One structure occurs as alternating weak and bright luminescent areas with features (<10 μm in size) growing perpendicular to the overgrowth's main growth direction (Figs. 4a, e and 5a). The second structure consists of irregularly shaped zones of alternating weak and bright CL (Figs. 4c and 5b). Such complex quartz overgrowth textures and distinct luminescent zonation have been described in various sandstones around the world (Fisher and Land, 1986; Suchecki and Bloch, 1988; Brint et al., 1991). The apparent variability of these features may simply result from how the grain was cut during thin-section preparation.

Examination of secondary electron (SE) images in conjunction with corresponding CL shows minor occurrences of pressure solution (<1 vol.%) in 65% of the thin sections. Fig. 4a–f shows examples of the typical degree of pressure solution in the samples. This small amount of pressure solution is not sufficient to form all of the silica cements in the shallowly buried St. Peter Sandstone, a conclusion also reached by Odom et al. (1979). It should be noted that both CL and SE images are needed to determine if pressure solution is present. For example, in SE, two grains in Fig. 4a and b appear to have undergone pressure solution; however, CL shows that the feature marked by an arrow in Fig. 4b is actually just an overgrowth growing into an adjacent overgrowth.

4.2. Oxygen isotopes

4.2.1. Laser fluorination

Laser fluorination analyses of 1–2 mg (100–150 grains at 150–300 μm diameter) samples of detrital quartz shows that $\delta^{18}O$ ranges from 9.6–10.4‰ (averaged values, $n \geqslant 2$). The average $\delta^{18}O$(DQ) value of these samples is 10.0 ± 0.2‰ (1SD, $n = 109$ for 53 rocks; Table 1, Fig. 6).

Whole quartz grain (WQG) samples, which include detrital quartz and overgrowths, were also analyzed. Averaged values ($n \geqslant 2$) of WQG samples range from 9.8‰ to 16.7‰ for the same 53 rocks ($n = 110$; Table 1, Fig. 6). Sixteen eolian samples have an average $\delta^{18}O$(WQG) value of 11.9 ± 1.3‰ (1SD, $n = 34$) excluding sample 04-WI-17B, which has an anomalous amount of cement compared to the other eolian samples. Eight marine samples have an average $\delta^{18}O$(WQG) value of 10.8 ± 0.4‰ (1SD, $n = 17$; Table 1).

Oxygen isotope analyses of whole rock samples from 18 rocks were made for comparison to WQG analyses. This was done to determine if the 150–300 μm diameter samples used in the $\delta^{18}O$(WQG) analyses contain a different amount of quartz cement than whole rock samples. It was found that whole rock samples give similar values to WQG samples (values are within 0.5‰ of each other, with one exception at 0.8‰; Table 1). Therefore, $\delta^{18}O$(WQG) values are a good representation for $\delta^{18}O$(WR). Hereafter and in Fig. 6, both sample types will be referred to as whole rock.

A plot of $\delta^{18}O$(WR) versus $\Delta^{18}O$(WR – DQ) shows a correlation between oxygen isotope ratios and the volume percent of quartz cement in each sample (Table 1, Fig. 7). It is shown below that this correlation indicates that samples with larger $\Delta^{18}O$(WR-DQ) and higher $\delta^{18}O$(WR) values have more quartz cement. Conversely, samples with $\delta^{18}O$(WR) values closest to $\delta^{18}O$(DQ) values represent rocks with little or no overgrowth.

4.2.2. Ion microprobe

Cathodoluminescence (CL) and secondary electron (SE) images were used in targeting spots for ion microprobe analysis. After ion microprobe analysis was complete, all analysis pits were examined by CL and SE to determine the exact nature of quartz analyzed: detrital quartz, quartz overgrowth, or a mixture. Mixed analyses (12% of analysis spots) are excluded from the following interpretation, but all analyses are shown in EA-2 along with textural assignment of detrital quartz, authigenic quartz overgrowth, and mixed analysis.

Values of $\delta^{18}O$(DQ) measured by ion microprobe range from 5.6‰ to 15.2‰ with an average of 10.0 ± 1.4‰ (1SD, $n = 91$ analyses of 12 samples; Fig. 8, EA-2). Oxygen isotope ratios of quartz overgrowths for 10 rocks (excluding two samples with dissolution features discussed below) give an average $\delta^{18}O$ value for all quartz cement of 29.3 ± 1.0‰ (1SD, $n = 161$; Fig. 8). The $\delta^{18}O$(cement) values for these 10 rocks are shown in histogram form in Fig. 9. The homogeneity of these results from widely spaced outcrops is consistent with the hypothesis that all quartz overgrowths in the shallowly buried St. Peter Sandstone formed from one continuous process.

Two samples with dissolution features (05-WI-29 and 05-WI-36) and physically detached, non-optically continu-

Table 1
Oxygen isotope ratios by laser fluorination for detrital quartz (DQ) grains, whole quartz grains (WQG), and whole rock (WR) analyses of the St. Peter Sandstone from SW Wisconsin and SE Minnesota

Sample name	Locality in Fig. 2	$\delta^{18}O$(DQ)[a]	$\delta^{18}O$(WQG)[b]	$\delta^{18}O$(WR)[c]	$\Delta^{18}O$[d]
Eolian samples					
04-WI-01	1	9.85	10.18		0.33
04-WI-02	1	9.95	11.53		1.58
04-WI-03[e]	2	9.91	10.58		0.67
04-WI-04	2	10.28	13.50		3.22
04-WI-04-2	2	10.13	13.65	13.90	3.52
04-WI-06A	4	9.98	10.64		0.67
04-WI-07	5	10.29	11.67	11.54	1.39
04-WI-08[f]	6	9.98	13.55		3.57
04-WI-08-2[f]	6	9.84	13.53		3.69
04-WI-09	7	9.83	9.76		−0.07
04-WI-10	7	9.61	10.35	11.21	0.74
04-WI-15	11	10.08	11.33	11.36	1.25
04-WI-16A	12	10.07	12.58	12.50	2.51
04-WI-17B	13	9.99	16.70	16.32	6.71
04-WI-17C	13	9.91	12.50	12.97	2.59
05-WI-37A	31	9.96	12.13	12.28	2.17
05-WI-38	32	10.24	12.61	12.28	2.38
			Ave = 11.9 ± 1.3‰, $n = 34$[g]	Ave = 12.3 ± 0.9‰, $n = 8$	
Marine samples					
04-WI-05	3	10.06	10.67		0.62
04-WI-12A	9	9.96	11.18	11.03	1.22
04-WI-13	9	9.83	10.56		0.73
04-WI-14	10	9.67	10.72	10.94	1.05
05-WI-28	22	10.15	11.30	11.33	1.15
05-WI-36	30	9.88	10.37	10.73	0.49
05-MN-45	39	9.84	10.31		0.47
05-WI-48	41	10.10	10.85	10.84	0.75
			Ave = 10.8 ± 0.4‰, $n = 17$	Ave = 11.0 ± 0.2‰, $n = 5$	
Depositional setting not determined					
04-WI-18	14	9.90	10.63		0.73
04-WI-19A	15	9.92	10.64		0.72
04-WI-20	15	9.83	10.79		0.96
04-WI-21	16	10.13	14.15		4.02
04-WI-21-2	16	10.22	13.54	13.09	3.32
04-WI-22	17	10.29	13.86		3.57
04-WI-23	18	10.32	12.91	13.11	2.59
04-WI-23-2	18	9.95	11.70		1.76
04-WI-24	19	10.25	13.70		3.45
04-WI-24-2	19	10.36	13.67	14.18	3.31
04-WI-25	20	10.02	13.41		3.39
05-WI-26A	21	10.01	10.73		0.72
05-WI-27	21	9.93	11.70		1.77
05-WI-29	23	10.03	10.36		0.33
05-WI-30	24	10.13	13.39	13.78	3.26
05-WI-31A	25	10.03	12.75		2.72
05-WI-32A	26	10.12	12.62		2.50
05-WI-33	27	10.12	10.36		0.24
05-WI-34A	28	10.26	11.06		0.81
05-WI-35	29	10.23	12.78		2.55
05-MN-39B	33	10.20	10.52		0.32
05-MN-40A	34	9.97	10.32		0.35
05-MN-41B	35	10.19	10.36		0.17
05-MN-42B	36	9.73	10.06		0.33
05-MN-43B	37	10.20	10.40		0.20
05-MN-44B	38	9.91	10.23		0.32

(*continued on next page*)

Table 1 (*continued*)

Sample name	Locality in Fig. 2	$\delta^{18}O(DQ)$[a]	$\delta^{18}O(WQG)$[b]	$\delta^{18}O(WR)$[c]	$\Delta^{18}O$[d]
05-MN-46	40	10.05	10.02		−0.03
05-MN-47	40	10.10	10.17		0.07
		Ave = 10.0 ± 0.2‰, $n = 109$			

All analyses are reported in standard ‰ notation relative to V-SMOW. All averages are given as one standard deviation.

[a] Analyses were made on 150–300 μm diameter grains treated with HF to dissolve quartz cement. Average of at least two analyses.

[b] Analyses were made on 150–300 μm diameter grains. Average of at least two analyses.

[c] Analyses were made on powdered samples and represent a single analysis except for sample 04-WI-17B, which is an average of two analyses.

[d] $\delta^{18}O(WR) - \delta^{18}O(DQ)$. This value correlates to the volume percent of quartz cement, where larger values correspond to more quartz cement. The negative values are within analytical uncertainty and represent <1 vol.% cement.

[e] All samples are from the Tonti Member, except this sample which is from the Readstown Member.

[f] Likely eolian according to Long (1988; see references).

[g] Excludes anomalous sample 04-WI-17B (see text, Section 4.2.1).

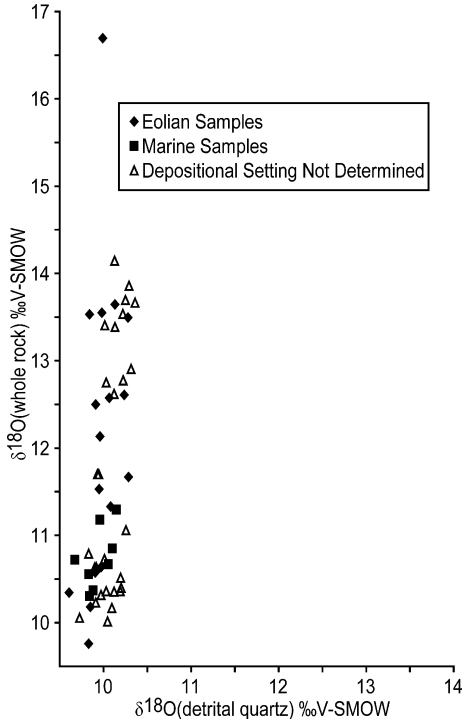

Fig. 6. Laser fluorination data for $\delta^{18}O$(whole rock) against $\delta^{18}O$(detrital quartz) for 53 rocks from the St. Peter Sandstone in SW Wisconsin and SE Minnesota differentiated by eolian, marine, and undetermined lithofacies. Whole rock samples are composed of both detrital quartz grains and quartz overgrowths.

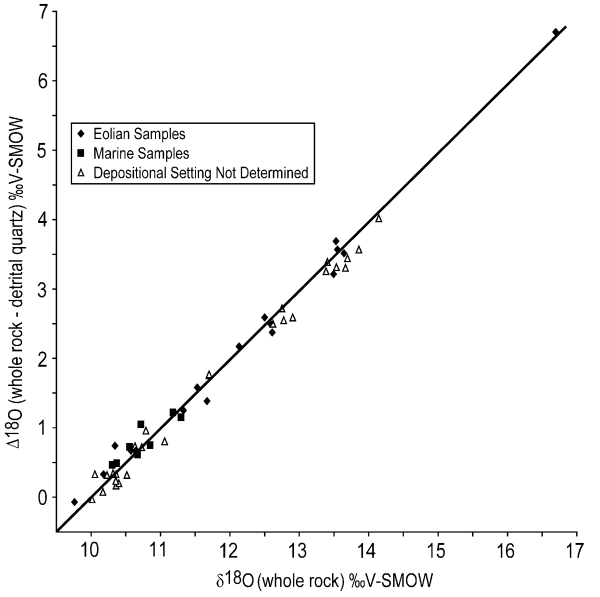

Fig. 7. Laser fluorination data for $\Delta^{18}O$(whole rock–detrital quartz) against $\delta^{18}O$(whole rock) for 53 rocks from the St. Peter Sandstone in SW Wisconsin and SE Minnesota differentiated by eolian, marine, and undetermined lithofacies. Samples with larger $\Delta^{18}O$ and $\delta^{18}O$(whole rock) values have more cement.

ous quartz overgrowths were analyzed by ion microprobe. These samples give detrital quartz values similar to all other samples in this study. However, the overgrowths in these samples have lower $\delta^{18}O$(cement) values (23.1–25.5‰; EA-2) compared to optically continuous quartz overgrowths. The $\delta^{18}O$(cement) values from these samples will not be used in the interpretation of the data given that they have formed or have been influenced by processes different from those acting on the rest of the samples in this study.

4.3. X-ray fluorescence (XRF) analysis

The concentration of eleven elements expressed as oxides for 24 whole rock samples is shown in Table 2. The following statistics refer only to Tonti Member samples of the St. Peter Sandstone. Samples have between 95.0 and 98.5 wt% SiO_2 and average 97.2 ± 0.9 wt% (1SD, $n = 23$). The range of compositional variation is: Al_2O_3, 0.12–1.03 wt %; K_2O, 0.01–0.84 wt%; Fe_2O_3, 0.10–1.44 wt%; MgO, 0.05–0.31 wt%; TiO_2, <0.01–0.04 wt%; CaO, <0.01–0.03 wt%; Na_2O, 0.02–0.10 wt%; Cr_2O_3,<0.10 wt%. MnO, and P_2O_5, were typically below detection limits. These findings are consistent with the mineralogy of the St. Peter Sandstone described by Odom et al. (1979) and the petrographic observations made in this study.

The X-ray fluorescence data do not indicate a correlation between any of the elements analyzed and the relative volume percent of quartz cement plotted as $\delta^{18}O(WR)$ shown in Electronic Annex EA-3. Furthermore, there is no statistical difference between marine and eolian samples.

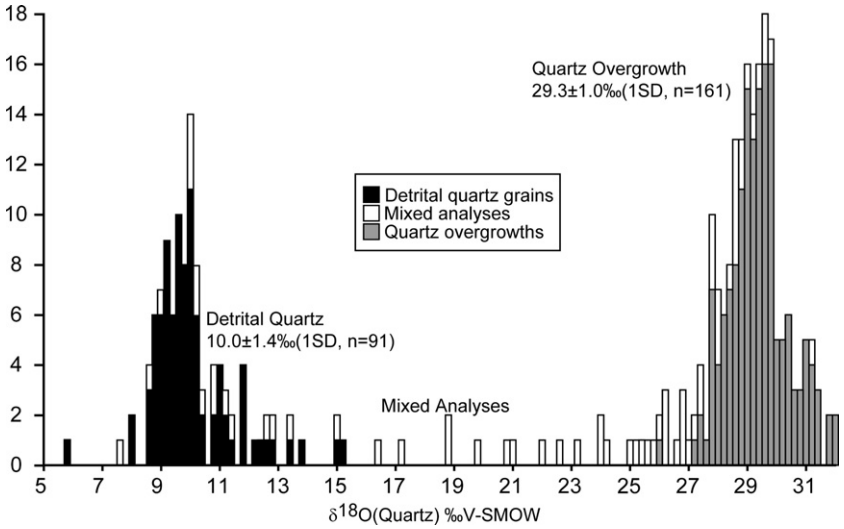

Fig. 8. Histogram showing the frequency of $\delta^{18}O$(quartz) from 6–10 μm-sized spots by ion microprobe. Mixed analyses are on the boundary of detrital quartz and quartz overgrowths. All analyses were conducted on samples from the St. Peter Sandstone from SW Wisconsin and SE Minnesota.

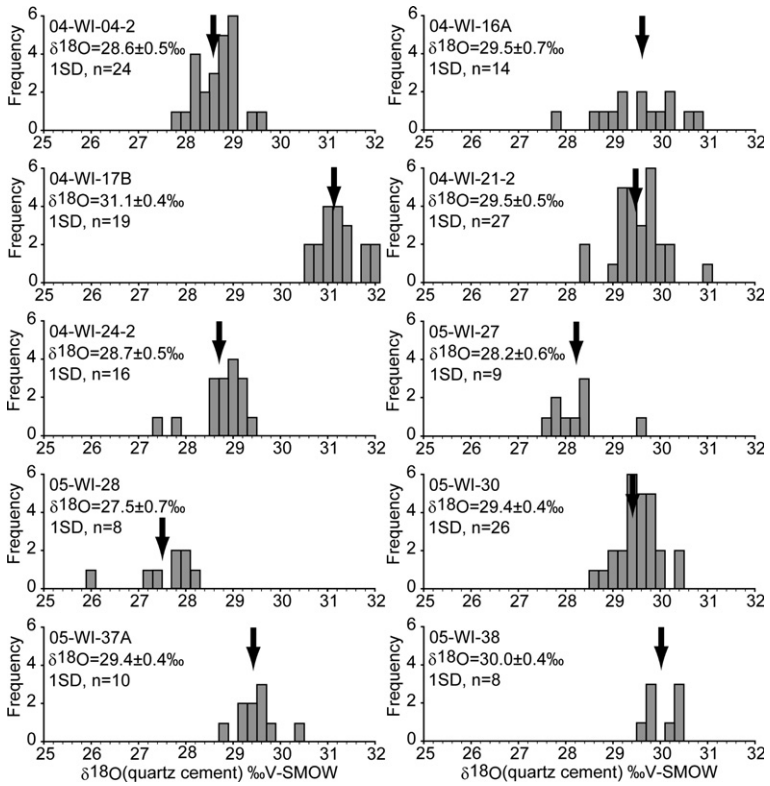

Fig. 9. Histograms of oxygen isotope ratios of quartz overgrowths in the St. Peter Sandstone from SW Wisconsin. All analyses are by ion microprobe. The arrows indicate the mean $\delta^{18}O$(cement) value of all analyses for each sample.

5. DISCUSSION

5.1. Comparison of laser fluorination and ion microprobe data for $\delta^{18}O$

Comparison of $\delta^{18}O$ values obtained by laser fluorination and by ion microprobe indicates the extent to which information has been averaged or lost by homogenization of the larger samples necessary for laser fluorination. Each laser fluorination analysis sampled 100–150 grains (1–2 mg) while the ion microprobe sampled <1 ng from a small portion of one grain. The narrow 0.8‰ range of average $\delta^{18}O$(DQ) per sample (Table 1, Fig. 6) suggests complete dissolution of quartz cement, however; the final test requires in situ analysis.

Table 2
X-ray fluorescence analyses for selected eolian and marine rocks of the St. Peter Sandstone from SW Wisconsin and SE Minnesota

Sample name	SiO_2	Al_2O_3	CaO	MgO	Na_2O	K_2O	Fe_2O_3	MnO	TiO_2	P_2O_5	Cr_2O_3	LOI[a]	Sum
Eolian samples from the Tonti Member													
04-WI-01	98.5	0.41	0.01	0.05	0.07	0.11	0.68	<0.01	0.03	<0.01	0.09	0.10	100.0
04-WI-02	97.4	0.55	0.03	0.06	0.07	0.20	1.44	0.01	0.03	<0.01	0.10	0.15	100.1
04-WI-04	97.9	0.75	0.03	0.06	0.09	0.21	0.77	<0.01	0.03	<0.01	0.08	0.15	100.1
04-WI-04-2	97.2	0.24	<0.01	0.15	0.02	0.15	0.17	<0.01	0.02	<0.01	<0.01	0.39	98.3
04-WI-06A	97.7	0.30	0.25	0.31	0.07	0.04	0.16	<0.01	0.03	<0.01	<0.01	0.85	99.8
04-WI-07	96.3	0.34	0.02	0.18	0.02	0.10	0.24	<0.01	0.02	<0.01	<0.01	0.54	97.8
04-WI-08-2[b]	97.5	0.51	0.12	0.22	0.05	0.09	0.14	<0.01	0.04	0.04	<0.01	0.70	99.4
04-WI-09[c]	95.0	0.24	<0.01	0.16	0.03	0.16	0.10	<0.01	0.02	<0.01	<0.01	0.54	96.3
04-WI-09[c]	97.4	0.23	<0.01	0.16	0.03	0.15	0.10	<0.01	0.02	<0.01	<0.01	0.16	98.3
04-WI-10	97.8	0.19	0.02	0.17	0.04	0.08	0.10	<0.01	0.04	<0.01	<0.01	0.50	99.0
04-WI-15	97.9	0.32	0.01	0.16	0.04	0.24	0.25	<0.01	0.04	<0.01	<0.01	0.45	99.4
04-WI-16A	95.3	0.13	<0.01	0.17	0.02	0.03	0.50	<0.01	0.02	0.01	<0.01	1.31	97.5
04-WI-17B	98.0	0.12	<0.01	0.16	0.05	0.01	0.14	<0.01	0.05	<0.01	<0.01	0.40	98.9
05-WI-37A	97.8	0.49	0.02	0.17	0.05	0.18	0.15	<0.01	0.05	<0.01	<0.01	0.60	99.5
05-WI-38	97.5	0.42	<0.01	0.16	0.02	0.11	0.15	<0.01	0.03	0.02	<0.01	0.69	99.1
Average	97.3	0.35	0.03	0.16	0.04	0.12	0.34	<0.01	0.03	<0.01	0.02		
1SD[d]	1.0	0.17	0.07	0.06	0.02	0.07	0.37	<0.01	0.01	0.01	0.04		
Eolian sample from the Readstown Member													
04-WI-03	76.7	1.02	5.97	3.66	0.26	0.23	0.86	0.01	0.09	0.24	<0.01	8.40	97.4
Marine samples from the Tonti Member													
04-WI-05	97.6	0.82	0.01	0.06	0.10	0.41	0.86	<0.01	0.03	<0.01	0.07	0.10	100.1
04-WI-12A	96.4	0.19	<0.01	0.16	0.03	0.15	0.16	<0.01	0.02	<0.01	<0.01	0.62	97.7
04-WI-13	97.6	0.30	0.02	0.19	0.04	0.17	0.11	<0.01	0.05	<0.01	<0.01	0.50	99.0
04-WI-14	96.8	0.32	<0.01	0.16	0.02	0.02	0.15	<0.01	0.03	<0.01	<0.01	0.39	97.9
05-WI-28	97.2	0.20	<0.01	0.16	0.05	0.13	0.23	<0.01	0.06	<0.01	<0.01	0.45	98.4
05-WI-36[e]	96.5	1.03	<0.01	0.15	0.03	0.84	0.10	<0.01	0.05	<0.01	<0.01	0.31	99.0
05-MN-45	98.2	0.47	0.01	0.17	0.05	0.04	0.15	<0.01	0.07	<0.01	<0.01	0.45	99.6
05-MN-48	97.1	0.33	<0.01	0.16	0.02	0.21	0.32	<0.01	0.06	<0.01	<0.01	0.46	98.6
Average	97.2	0.46	0.01	0.15	0.04	0.25	0.26	<0.01	0.05	<0.01	0.01		
1SD[d]	0.6	0.31	0.01	0.04	0.03	0.27	0.25	<0.01	0.02	<0.01	0.02		

Detection limits are 0.01 wt% for all oxides except Na_2O which is 0.02 wt% and MgO which is 0.03 wt%.
[a] LOI, lost on ignition.
[b] Likely eolian according to Long (1988; see references).
[c] This sample was submitted as a blind duplicate to determine the internal precision of the analyses.
[d] One standard deviation.
[e] Sample with non-optically continuous quartz overgrowths.

The oxygen isotope analyses by ion microprobe show that $\delta^{18}O(DQ)$ ranges from 7.9–15.2‰ (EA-2). These values are far more variable than suggested by the laser fluorination analyses, which homogenized at least 100 sand grains per analysis. Thus, only the ion microprobe data reveal the true variability of detrital quartz, confirming that most of the quartz originally derived from a mixture of dominantly igneous sources. A value of $\delta^{18}O(quartz) = 10‰$ would represent a whole rock value of about 9‰ for typical granitic rocks of the protolith. The higher $\delta^{18}O$ ion microprobe values (above 12‰) suggest that some detrital quartz grains originally derived from metamorphic sources, and that there is no systematic difference in the source region discernable with oxygen isotope composition. While the in situ analyses reveal the true variability of each sample, the average $\delta^{18}O(DQ)$ measured by ion microprobe ($10.1 \pm 1.4‰$, 1SD, $n = 91$) is in perfect agreement with the average laser fluorination $\delta^{18}O$ value of $10.1 \pm 0.2‰$ (1SD; $n = 27$) for the same twelve rocks (Table 3). There is no systematic difference between the results of these two methods (Table 3).

5.2. Comparison of oxygen isotope data from previous research

Graham et al. (1996) measured oxygen isotope ratios by ion microprobe for St. Peter Sandstone samples from the Wisconsin Dome and found that $\delta^{18}O(DQ)$ ranges from 5.4‰ to 12.7‰. However, the single-collector ion microprobe used in 1996 study had a much larger spot size (20–30 μm) compared to the new multi-collector ion microprobe (6–10 μm) in this study. Furthermore, the analytical precision attained by the single-collector ion microprobe (±1‰, 1SD) is not as good as the precision attained by

Table 3
Comparison of $\delta^{18}O$(detrital quartz) by ion microprobe and laser fluorination for samples of the St. Peter Sandstone from SW Wisconsin

Sample name	$\delta^{18}O$ by ion microprobe	Number of analyses	$\delta^{18}O$ by laser fluorination	Number of analyses
Eolian samples				
04-WI-16A	9.6	5	10.0	2
04-WI-17B	9.2	4	10.0	2
05-WI-28	11.0	7	10.2	3
05-WI-36	9.0	4	9.9	2
Marine samples				
04-WI-04-2	10.0	7	10.3	2
05-WI-37A	9.5	12	10.0	4
05-WI-38	10.0	8	10.2	2
Depositional setting not determined				
04-WI-21-2	10.3	11	10.2	2
04-WI-24-2	10.1	12	10.4	2
05-WI-27	10.2	9	9.9	2
05-WI-29	9.8	4	10.0	2
05-WI-30	10.1	8	10.1	2
	Ave = 10.1 ± 1.4‰, $n = 89$		Ave = 10.1 ± 0.2‰, $n = 27$	

All analyses are reported in standard ‰ notation relative to V-SMOW. All averages are given as one standard deviation.

the multi-collector ion microprobe (⩽0.2‰, 1SD). Thus, the 1996 values agree within analytical uncertainty to the $\delta^{18}O$(DQ) values of 7.9–15.2‰ in this study.

Ten samples in this study have $\delta^{18}O$(cement) values from 25.9–32.0‰ (EA-2) that are in good agreement with the earlier study that found $\delta^{18}O$(cement) from two Wisconsin samples varies from 17.7–31.6‰ (Graham et al., 1996). The larger range of values in the 1996 data is likely due to poorer precision, larger spot size, and failure to identify mixed analyses that included both quartz cement and detrital grains.

5.3. Cathodoluminescence (CL) textures and oxygen isotope data

Despite the complexity of the quartz overgrowths, and regardless of the development stage of the overgrowths in the St. Peter Sandstone, the differences in the average oxygen isotope values seen in Fig. 9 are small, less than 4‰. A similar situation in which complex luminescent zonation within quartz overgrowths gives small variation in oxygen isotope values has been observed by Sullivan et al. (1997) from an eolian sandstone in the Leman gas field (North Sea).

5.4. Calculation of volume percent quartz overgrowth

Oxygen isotope ratios of whole rock, detrital quartz, and quartz cement allow calculation of the volume percent of quartz overgrowth present in each sample by mass balance. Previous studies have estimated the amounts of cement (Milliken et al., 1981; Fisher and Land, 1986; Brint et al., 1991; Girard and Deynoux, 1991; Webb and Golding, 1998), but in the absence of in situ analyses, the $\delta^{18}O$(cement) was uncertain. This study uses the new ion microprobe data to measure directly the $\delta^{18}O$(cement) and shows that it is homogeneous. Thus, the volume percent of cement can be calculated with certainty that was not previously possible.

The volume percent of quartz cement in all samples was calculated using two different $\delta^{18}O$(cement) values. Method 1 uses the $\delta^{18}O$(cement) value averaged together from all ten samples, while Method 2 uses the $\delta^{18}O$(cement) averaged for each individual sample analyzed by ion microprobe. The difference between these two values is less than 1.8‰. The first method uses the average $\delta^{18}O$(cement) = 29.3‰ (Fig. 8), the average $\delta^{18}O$(DQ) by laser fluorination for each sample (Table 1), and the $\delta^{18}O$(WR) value listed in Table 1 for each of the 53 rocks (Method 1 in Table 4). This calculation shows that quartz cement varies from <1 to 21 vol.% with one outlier (sample 04-WI-17B) at 35 vol.% cement (Table 4). This outlier is significantly cemented by quartz and typically has between six and eleven growth zones (visible by CL) around a single detrital quartz grain (Fig. 4). This sample was collected from Gibraltar Rock, a prominent erosional remnant that is highly cemented and reflects local diagenetic processes different from those acting on the rest of the St. Peter Sandstone from this study area.

The volume percent of quartz cement was also calculated for 10 rocks analyzed by ion microprobe using the average $\delta^{18}O$(cement) for each sample (Fig. 9), the average $\delta^{18}O$(DQ) by laser fluorination for each sample (Table 1), and the average $\delta^{18}O$(WR) value listed in Table 1 for each sample (Method 2 in Table 4). The volume percent of cement from this calculation for all 10 rocks is similar to the values calculated by Method 1 and yields 32 vol.% cement for the anomalous sample 04-WI-17B. This is a more accurate cement estimate for this sample given that Method 2 used the actual $\delta^{18}O$(cement) value of 31.1‰, almost 2‰ higher than the average of all samples. Values for such large volume percent cement have been reported for various silcretes and sandstones by Dutton and Diggs (1990), Murray (1990), Girard and Deynoux (1991), and Alexandre et al. (2004).

Comparison of the calculated volume percent of quartz cement in known eolian and marine samples shows an average of 10–14 vol.% cement in eolian samples, excluding

Table 4
Volume percent of quartz cement in SW Wisconsin and SE Minnesota samples from the St. Peter Sandstone calculated using mass balance of whole rock, detrital quartz, and quartz overgrowth oxygen isotope ratios (see text, Section 5.4)

Sample name	Vol.% Method 1[a]	Vol.% Method 2[b]	Sample name	Vol.% Method 1[a]	Vol.% Method 2[b]
Eolian samples			*Depositional setting not determined*		
04-WI-01	2		04-WI-18	4	
04-WI-02	8		04-WI-19A	4	
04-WI-03[c]	3		04-WI-20	5	
04-WI-04	17		04-WI-21	21	
04-WI-04-2	18	19	04-WI-21-2	17	17
04-WI-06A	3		04-WI-22	19	
04-WI-07	7		04-WI-23	14	
04-WI-08[d]	18		04-WI-23-2	9	
04-WI-08-2[d]	19		04-WI-24	18	
04-WI-09	<1		04-WI-24-2	17	19
04-WI-10	4		04-WI-25	18	
04-WI-15	7		05-WI-26A	4	
04-WI-16A	13	13	05-WI-27	9	10
04-WI-17B	35	32	05-WI-29	2	
04-WI-17C	13		05-WI-30	17	17
05-WI-37A	11	11	05-WI-31A	14	
05-WI-38	12	12	05-WI-32A	13	
Average[e]	10%	14%	05-WI-33	1	
Marine samples			05-WI-34A	4	
04-WI-05	3		05-WI-35	13	
04-WI-12A	6		05-WI-39B	2	
04-WI-13	4		05-MN-40A	2	
04-WI-14	5		05-MN-41B	1	
05-WI-28	6	7	05-MN-42B	2	
05-WI-36	3		05-MN-43B	1	
05-MN-45	2		05-MN-44B	2	
05-WI-48	4		05-MN-46	<1	
Average	4%		05-MN-47	<1	

[a] Calculated using the average $\delta^{18}O$(DQ) for each sample, the average $\delta^{18}O$(WR) for each sample, and the average $\delta^{18}O$(cement) for all samples of 29.3‰.
[b] Calculated using the average $\delta^{18}O$(DQ) for all samples, the average $\delta^{18}O$(WR) for each sample, and the average $\delta^{18}O$(cement) for each sample.
[c] All samples are from the Tonti Member, except this sample, which is from the Readstown Member.
[d] Sample is likely eolian according to Long (1988; see references).
[e] Average excludes sample 04-WI-17B given its abnormal amount of cement relative to the other samples.

sample 04-WI-17B (32 vol.%), compared to 4 vol.% cement in marine samples (Table 4). The differing volume percent cement in eolian and fluvial sands may result from local variability or from waters with different silica compositions responsible for overgrowth formation. Marine samples may also have more clay coating detrital quartz grain boundaries, which can retard and/or inhibit overgrowth formation (Odom et al., 1979; McBride, 1989; Dutton and Diggs, 1990).

5.5. Intergranular volume and burial depth

Intergranular volume (IGV) is the sum of intergranular pore space, intergranular cement and depositional matrix. Intergranular volume was calculated for all samples analyzed by ion microprobe because IGV can be related to the degree of compaction and burial depth (Table 5; Paxton et al., 2002). Intergranular pore space was calculated from at least two representative secondary electron (SE) images of each sample using the public domain image processing and analysis program, NIH Image. NIH Image easily distinguishes between porosity (which is black in the images) and detrital quartz and quartz overgrowths (light gray), yielding the percentage of intergranular pore space and the percentage of quartz in the image (i.e. detrital quartz plus quartz overgrowths). See Fig. 4b, d, and f for examples of color differences between porosity (epoxy) and quartz. The percentage of quartz cement was calculated using mass balance of oxygen isotopes (Method 2 in Table 4). The percentage of depositional matrix is judged to be not significant since the St. Peter Sandstone in SW Wisconsin is a clean quartz arenite and the thin sections show little to no depositional matrix. This calculation should be accurate to within 2%. Furthermore, a check of the internal consistency of the results is available from the samples collected in the Upper Mississippi Valley lead–zinc district. These

Table 5
Intergranular Volume (IGV) for SW Wisconsin St. Peter Sandstone samples analyzed by ion microprobe

Sample name	Percent porosity	Percent cement	Intergranular volume (IGV)	Sample location
04-WI-04-2	12	19	31	SE part of study area
04-WI-16A	12	13	25	Central part of study area
04-WI-17B	8	32	40	NE part of study area
04-WI-24-2	10	19	29	UMV District[a]
05-WI-21-2	12	17	29	UMV District[a]
05-WI-27	12	10	22	UMV District[a]
05-WI-28	22	7	29	UMV District[a]
05-WI-30	11	17	28	UMV District[a]
05-WI-37A	13	11	24	NW part of study area
05-WI-38	14	12	26	NW part of study area

Percent porosity was calculated using NIH image (see text Section 5.5). Percent cement values are from Method 2 in Table 4 (see text Section 5.4).
[a] Samples from the Upper Mississippi Valley lead–zinc district.

samples give similar IGV values of 28 and 29 (excluding sample 05-WI-27) despite varying amounts of cement from 7 to 19%.

The results in Table 5 confirm a shallow burial depth for the St. Peter Sandstone based on the intergranular compaction curve of Paxton et al. (2002). This conclusion is supported by the $\delta^{18}O$ of quartz cements measured in this study and by Graham et al. (1996). As discussed earlier, the higher temperatures experienced by deeply buried St. Peter Sandstone caused values of $\delta^{18}O$ (quartz overgrowths) to average 13‰ lower than those measured here.

5.6. Meteoric water vs. MVT hydrothermal brines

5.6.1. General considerations for the temperature models

Oxygen isotope ratios in quartz overgrowths preserve information about the temperatures and compositions of fluids from which the quartz cement formed. Thus, the temperatures of overgrowth formation can be determined if fluid composition is known or conversely, fluid composition can be calculated if temperature is independently known. In this study, the oxygen isotope compositions of water in equilibrium with quartz were calculated (Fig. 10; Clayton et al., 1972) over the possible range of overgrowth formation temperatures, which are from 10 to 110 °C. This range spans estimates from a normal conductive geothermal gradient for the study area, fluid inclusion data from the Upper Mississippi Valley lead–zinc mineral district (McLimans, 1977), and the brine migration model of Arnold et al. (1996).

Two models of quartz overgrowth formation are discussed: (1) high temperature (50–110 °C) formation from migrating MVT brines and (2) low temperature (10–30 °C) formation at near-surface conditions. Variations of each model include the scale of temperature variation and variability of $\delta^{18}O$(water).

Any model for the genesis of quartz overgrowths in the St. Peter Sandstone should consider the following observations. The sandstone is a super mature quartz arenite, averaging 97% SiO_2. The maximum burial depths of the sandstone were <1 km. The volume percent of quartz cement in the study area averages 9% and porosity is ubiquitous. The overgrowths are syntaxial on detrital quartz grains. The fluid flow model of Arnold et al. (1996) predicts that MVT brines flowed northward through the St. Peter Sandstone causing a regional temperature variation from 110 °C near the Illinois border to 50 °C at the northern end of the study area. At 100 °C, the MVT brines range in $\delta^{18}O$ composition from +2‰ to +3‰ (Sverjensky, 1981). Finally, the new ion microprobe data show that quartz overgrowths are homogeneous in $\delta^{18}O$ at 29.3 ± 1‰ (1SD, $n = 161$).

5.6.2. High temperature models

The hypothesis of regional variation in temperature during quartz overgrowth formation can be evaluated with the new oxygen isotope data. The model of MVT fluids envisioned by Arnold et al. (1996) predicts that overgrowths increase in $\delta^{18}O$ by about 9‰ if fluid composition is approximately constant and temperatures decrease from 110 °C in the south to 50 °C in the north. The differences in the average oxygen isotope values seen in Fig. 9 are small, less than 4‰, and are much less than would be predicted by this hydrothermal flow model. Thus, the new ion microprobe data show that no regional variation of $\delta^{18}O$ of quartz overgrowths exists, and clearly disprove this model.

Alternatively, if the $\delta^{18}O$ of circulating waters decrease as they flow from south to north, in perfect synchronization with dropping temperature, it would, in theory, be possible to precipitate overgrowths with constant $\delta^{18}O$. However, this scenario would require a very fortuitous set of circumstances for which there is no physical explanation and is highly unlikely. Furthermore, at 100 °C, the quartz overgrowths that have $\delta^{18}O = 29.3$‰ would have formed from water with a $\delta^{18}O$ composition of 8‰. This is in disagreement with the 2–3‰ oxygen isotopic composition of the water calculated by Sverjensky (1981). Thus, such perfectly correlated regional variations in temperature and $\delta^{18}O(H_2O)$ are not reasonable for overgrowth formation.

A third high temperature model-with temperatures of ~110 °C and constant $\delta^{18}O(H_2O)$ values of approximately +9‰ (Fig. 10) could be possible. However, the modeling of Arnold et al. (1996) was not able to create this situation due to conductive and advective losses of heat through overlying strata given a boundary condition that temperatures were 20 °C at the surface throughout the study area. The model of Arnold et al. (1996) generates the isotherms shown in Fig. 2 assuming a reasonable flow rate of 10 m/

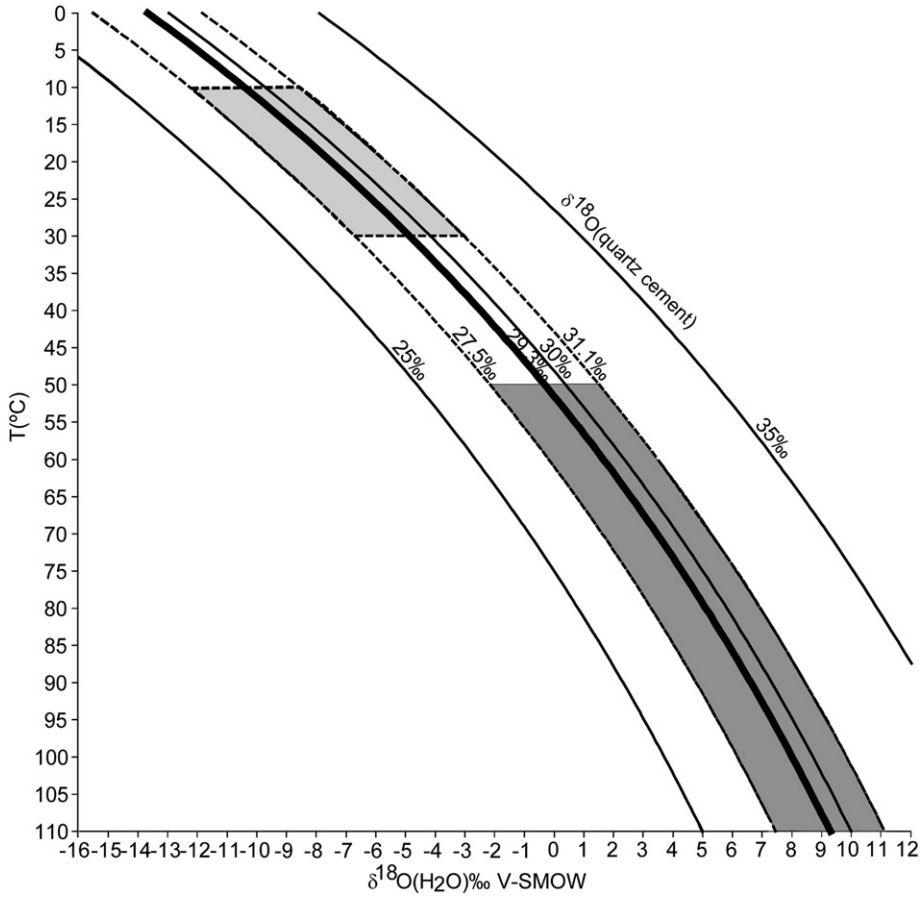

Fig. 10. Plot of $\delta^{18}O$(water) in equilibrium with quartz cement ($\delta^{18}O(Qt) = 25‰$, 30‰, and 35‰, contours) as a function of temperature (Clayton et al., 1972). The thicker line indicates the average $\delta^{18}O$ of 29.3‰ for quartz cements in ten samples analyzed by ion microprobe. The dashed quartz cement curves (27.5 and 31.1‰) represent the minimum and maximum average $\delta^{18}O$(cement) value for the 10 samples analyzed by ion microprobe given in Fig. 9. The light gray box outlines the $\delta^{18}O$(water) composition and temperature range for the low temperature model (10–30 °C) given the data from this study, while the dark gray box outlines the high temperature quartz overgrowth formation model (50–110 °C).

year at the southern border of the study area. Given that these aquifers were shallow, poorly insulted, and locally venting to the surface, it is not reasonable to propose that fluid flow could have maintained temperatures of ~100 °C throughout the study area, which extends well to the north of areas with economic concentrations of lead and zinc mineralization. Thus, we conclude that the overgrowths did not form by heated brines at a constant temperature of ~100 °C associated with the MVT ore deposits.

5.6.3. Low temperature models

Since the higher temperature quartz overgrowth formation models are not consistent with the new ion microprobe data, the lower temperature models must be explored. Meteoric water with a nearly constant temperature and $\delta^{18}O(H_2O)$ composition throughout the study area constitutes a reasonable fluid to hypothesize for the precipitation of quartz cements in a near surface environment. In this model, either downward-moving surface fluids (vadose or phreatic) or upward-moving fluids (phreatic) could be responsible for quartz overgrowth formation. Along a normal conductive geothermal gradient (20 to 30 °C/km), quartz cementation would occur in the temperature range of 10–30 °C at depths of <1 km (Bethke, 1986).

The extreme homogeneity of $\delta^{18}O$(cement) values found in this study strongly suggests that they formed in a uniform environment and that there was little variability in either the $\delta^{18}O$ of groundwater or temperature. At one extreme, if temperature was constant then the maximum variability of water is suggested to have been ±1‰. Alternatively, if $\delta^{18}O(H_2O)$ was constant (varying by $< \pm 1.0‰$) then temperature varied by less than ±5 °C. Such uniform conditions argue against a dynamic flowing system and suggest the overgrowths formed as shallow cements, most likely in the vadose zone at 10–30 °C.

The composition of water in equilibrium with the average quartz cements is −10‰ at 10 °C and −5‰ at 30 °C (Fig. 10). Quartz overgrowths forming in a near-surface environment would have formed during or shortly after deposition of the St. Peter Sandstone. If this is correct, the study area would have been located closer to equatorial latitudes (McElhinny, 1973; McElhinny and Opdyke, 1973) than its current position at 40°N. Since the $\delta^{18}O$ values of meteoric water vary with latitude, meteoric water responsi-

ble for overgrowth formation between the equator and 40°N would range from nearly −12‰ to −3‰ (closer to −3 for the equator; IAEA, 1981) at low elevation where quartz sedimentation is likely near to the ocean. These values are in agreement with the fluid compositions (−10‰ to −5‰) responsible for a constant $\delta^{18}O$(cement) of 29.3‰. These estimates support the interpretation that quartz overgrowths formed as silcretes in a near-surface environment most likely at temperatures of 10–30 °C.

5.7. Silcrete

The silcrete cements in the St. Peter Sandstone are best characterized as forming above the water table by evaporation in a near-surface environment. The high evaporation rates in the arid to semi-arid climates during or shortly after deposition of the eolian sands also point to this conclusion. It should be noted that the average $\delta^{18}O$ values for cements in marine and eolian sandstones are similar. This might suggest that marine cements formed in the near shore environment dominated by fresh water, or that these cements formed during periods of marine lowstand.

Quartz cements, syntaxial or otherwise, in silcretes are generally described as forming in association with microquartz, chalcedony, and/or opaline silica (Smale, 1973; Summerfield, 1983a). Although Hoholick et al. (1984) described chalcedony in the St. Peter Sandstone, fibrous cements are uncommon, and none were seen in this study.

The general preservation of metastable silica cements may be attributed to the rarity of recrystallizing them at low temperatures (Summerfield, 1983a). For example, Goldstein and Rossi (2002) propose that it takes temperatures over 180 °C to recrystallize fibrous quartz. Thus, the syntaxial cements reported in the study likely precipitated as syntaxial cements. They are not recrystallized opaline or microcrystalline silica.

5.8. Can quartz overgrowths form at low temperatures?

It is commonly thought that metastable silica cements should form at low temperatures and that syntaxial quartz overgrowths require higher temperatures to form (Bjorlykke and Egeberg, 1993). However Williams and Crerar (1985) show that the precipitation of equilibrated quartz overgrowths is favored by slow processes from fluids that are close to quartz saturation. Metastable cement formation is favored by high degrees of silica oversaturation such as are common in the presence of volcanic glass or diagenetic reactions. Thus the precipitation of syntaxial cements is favored in clean supermature quartz arenites such as the St. Peter Sandstone and temperature is not the only control on the growth of quartz.

The processes favoring low temperature syntaxial cements are well understood. First, the concentration of silica and foreign ions in formation waters will cause the nucleation and precipitation rates of SiO_2 to vary (Summerfield, 1983a,b; Williams and Crerar, 1985; Thiry and Millot, 1987; Thiry and Milnes, 1991). High concentrations of silica and foreign ions will cause faster nucleation and precipitation rates, favoring abundant nuclei and fine-grained quartz (Folk and Pittman, 1971; Summerfield, 1983b; Williams and Crerar, 1985; Murray, 1990; Thiry and Milnes, 1991). Conversely, low levels of silica concentration and foreign ions will favor quartz cementation (Summerfield, 1983a,b; Williams and Crerar, 1985; Murray, 1990; Thiry and Milnes, 1991). Furthermore, once nucleated, quartz overgrowths are likely to continue scavenging silica, promoting their continued formation (Pittman, 1972; Austin, 1974; Bjorlykke and Egeberg, 1993).

Low temperature syntaxial quartz cements have been reported in several studies. For example, Mackenzie and Gees (1971) showed that precipitation of quartz from an aqueous solution is possible at 20 °C. Furthermore, Hervig et al. (1995) studied diagenetic quartz from Mississippian sandstones of the western Canadian sedimentary basin by ion microprobe and found that the authigenic cements typically range in $\delta^{18}O$ from 20‰ to 34‰ for currently deeply buried (>1.6 km) samples. The authors concluded that the cements may have precipitated from meteoric water at temperatures between 15 and 35 °C near the basin center. Similarly, Girard and Deynoux (1991) used oxygen isotopic evidence to conclude that quartz cements in West African upper Proterozoic quartzites precipitated at temperatures between 0 and 50 °C from meteoric water. Alexandre et al. (2004) investigated one sample from the Lake Eyre Basin (Australia) and found that silcrete cement is composed predominantly of cryptocrystalline quartz (23%), followed by microcrystalline quartz (6%) and optically continuous quartz overgrowths (4%), which did not display any signs of dissolution features or embayments. The $\delta^{18}O$(cement) value calculated by Alexandre et al. (2004) for this sample ranges between 24.8‰ and 25.8‰. The authors hypothesize that this sample formed between 15 and 20 °C from $\delta^{18}O(H_2O)$ between −6.9‰ and −12.2‰ as a silcrete.

The porosity of the sands undergoing cementation influences the type of silica cement formed. Low porosity restricts fluid flow, promoting slower nucleation and growth rates, and the precipitation of quartz (Folk and Pittman, 1971; Summerfield, 1983a; Thiry and Milnes, 1991). Furthermore, the most permeable parts of a sandstone may receive the most quartz cement, causing the newly cemented areas to gradually become less permeable (Murray, 1990; Bjorlykke and Egeberg, 1993; Sullivan et al., 1997).

Small amounts of syntaxial cement might precipitate in porous sandstones at deeper groundwater levels in the phreatic zone; however, precipitation of authigenic cements is favored by evaporation, which can only occur at or above the water table. The vadose zone is potentially a more homogeneous environment; the homogeneity of the oxygen isotopes in the cements of the St. Peter Sandstone shows that neither temperature nor water composition changed significantly. Unless there was some extremely unlikely coincidence, the variation of water was less than ±2‰ (if temperature was constant) or the variation of temperature was less than ±6 °C (if water composition was constant). The temperature of the vadose zone should reflect mostly depth and climate. In contrast, if circulating ground waters in the phreatic zone precipitated quartz cements, variations in temperature, water composition, or both would result in variable $\delta^{18}O$(cement). As a second consideration, evapora-

tion in the vadose zone is a good mechanism for precipitation of cements (fractionation by evaporation might be small and constant), while precipitation of cements in a water-saturated rock would require a reaction, mixing of fluids or a change in temperature with attendant variability in $\delta^{18}O$.

6. CONCLUSIONS

CL imaging shows that quartz overgrowths with complex luminescent zonation are common in the shallowly buried St. Peter Sandstone on the Wisconsin Dome. Despite the complexity of these overgrowths, in situ oxygen isotope ratios are remarkably similar, averaging $\delta^{18}O = 29.3 \pm 1.0‰$ (1SD, $n = 161$). These $\delta^{18}O$ values suggest that a similar environment was responsible for the formation of all textural varieties of overgrowth that are seen on a thin section and on a regional scale.

The volume percent of quartz cement can be estimated in this study from a single inexpensive oxygen isotope analysis of a whole rock sample because the average $\delta^{18}O(DQ)$ values are similar and the $\delta^{18}O(cement)$ values are constant throughout the study area. This is a much quicker approach than point counting samples to determine the volume percent of cement in each sample. Furthermore, the isotopic analyses average a larger, more representative volume of sample than just a small area of a thin section. Quartz cement in most samples of the St. Peter Sandstone varies from <1 to 21 vol.%. Eolian samples have an average of 10–14 vol.% cement compared to marine samples, which have 4 vol.% cement.

The homogeneity of $\delta^{18}O(cement)$ is best explained if quartz overgrowths formed in a shallow near-surface environment. To our knowledge, this study is the first report of syntaxial quartz overgrowths that are interpreted as silcretes formed in a low temperature, near surface environment in the absence of microquartz chalcedony, or opaline silica. These quartz cements would form from meteoric water with a $\delta^{18}O(H_2O)$ composition between $-10‰$ and $-5‰$ at temperatures between 10 and 30 °C as silcretes.

ACKNOWLEDGMENTS

Mike Spicuzza assisted in operation of the Wisconsin Stable Isotope Laboratory. Thin sections were made by Brian Hess. Bob Dott, Charlie Byers, Jean Bahr, and Clint Cowan assisted with conversations and sample collection. Bruce Selleck and William Peck (Colgate University) provided assistance with SEM imaging. John Fournelle, Aaron Cavosie, and Zeb Page assisted with CL imaging. Mary Diman helped to draft and prepare figures. Constructive reviews by Dimitri Sverjensky, Martin Appold, and Stan Paxton improved this manuscript. This project was funded by DOE (93ER14389). The Wisc-SIMS Ion Microprobe lab is funded by NSF (EAR-0319230).

APPENDIX A. SUPPLEMENTARY DATA

Supplementary data associated with this article can be found, in the online version, at doi:10.1016/j.gca.2007.05.014.

REFERENCES

Alexandre A., Meunier JD., Llorens E., Hill S. M. and Savin S. M. (2004) Methodological improvements for investigating silcrete formation: petrography, Ft-IR and oxygen isotope ratio of silcrete quartz cement, Lake Eyre Basin (Australia). *Chem. Geol.* **211**, 261–274.

Arnold B. W., Bahr J. M. and Fantucci R. (1996) Paleohydrogeology of the Upper Mississippi Valley zinc–lead district. In *Carbonate-hosted lead–zinc deposits*. (ed. D. Sangster). Soc. Econ. Geol. 4, pp. 378–389.

Austin G. S. (1974) Multiple overgrowths on detrital quartz sand grains in the Shakopee Formation (Lower Ordovician) of Minnesota. *J. Sed. Petrol.* **44**, 358–362.

Bailey S. W. and Cameron E. N. (1951) Temperatures of mineral formation in bottom-run lead–zinc deposits of the Upper Mississippi Valley, as indicated by liquid inclusions. *Econ. Geol.* **46**, 626–651.

Bethke C. M. (1986) Hydrologic constraints on the genesis of the Upper Mississippi Valley mineral district from Illinois Basin brines. *Econ. Geol.* **81**, 233–249.

Bjorlykke K. and Egeberg P. K. (1993) Quartz cementation in sedimentary basins. *Am. Assoc. Petrol. Geol. Bull.* **77**, 1538–1548.

Brannon J. C., Podosek F. A. and McLimans R. K. (1992) Alleghenian age of the Upper Mississippi Valley zinc–lead deposit determined by Rb–Sr dating of sphalerite. *Nature* **356**, 509–511.

Brint J. F., Hamilton P. J., Haszeldine R. S., Fallick A. E. and Brown S. (1991) Oxygen isotopic analysis of diagenetic quartz overgrowths from the Brent Sands: a comparison of two preparation methods. *J. Sed. Petrol.* **61**, 527–533.

Clayton R. N., O'Neil J. R. and Mayeda T. K. (1972) Oxygen isotope exchange between quartz and water. *J. Geophys. Res.* **77**, 3057–3067.

Dapples E. C. (1955) General lithofacies relationship of St. Peter Sandstone and Simpson Group. *Am. Assoc. Petrol. Geol. Bull.* **39**, 444–467.

Drzewiecki P. A., Simo J. A., Brown P. E., Castrogiovanni E., Nadon G. C., Shepherd L. D., Valley J. W., Vandrey M. R., Winter B. L. and Barnes D. A. (1994) Diagenesis, diagenetic banding, and porosity evolution of the Middle Ordovician St. Peter Sandstone and Glenwood Formation in the Michigan Basin. In *Basin Compartments and Seals* (ed. P. J. Ortoleva). Am. Assoc. Petrol. Geol. Mem. 61, pp. 179–199.

Dutton S. P. and Diggs T. N. (1990) History of quartz cementation in the Lower Cretaceous Travis Peak Formation, East Texas. *J. Sed. Petrol.* **60**, 191–202.

Fisher R. S. and Land L. S. (1986) Diagenetic history of Eocene Wilcox sandstones, South-Central Texas. *Geochim. Cosmochim. Acta* **50**, 551–561.

Folk R. L. and Pittman J. S. (1971) Length-slow chalcedony: a new testament for vanished evaporites. *J. Sed. Petrol.* **41**, 1045–1058.

Garven G. and Freeze R. A. (1984a) Theoretical analysis of the role of groundwater flow in the genesis of stratabound ore deposits: 1, mathematical and numerical model. *Am. J. Sci.* **284**, 1085–1124.

Garven G. and Freeze R. A. (1984b) Theoretical analysis of the role of groundwater flow in the genesis of stratabound ore deposits: 2, quantitative results. *Am. J. Sci.* **284**, 1125–1174.

Garven G., Ge S., Person M. A. and Sverjensky D. A. (1993) Genesis of stratabound ore deposits in the Midcontinent basins of North America: 1, the role of regional groundwater flow. *Am. J. Sci.* **293**, 497–568.

Girard J. P. and Deynoux M. (1991) Oxygen isotope study of diagenetic quartz overgrowth from Upper Proterozoic quartzites of western Mali, Taoudeni Basin: implication for conditions of quartz cementation. *J. Sed. Petrol.* **61**, 406–418.

Goldstein R. H. and Rossi C. (2002) Recrystallization in quartz overgrowths. *J. Sed. Res.* **72**, 432–440.

Graham C. M., Valley J. W. and Winter B. L. (1996) Ion microprobe analysis of $^{18}O/^{16}O$ in authigenic and detrital quartz in the St. Peter Sandstone, Michigan Basin and Wisconsin Arch, USA: contrasting diagenetic histories. *Geochim. Cosmochim. Acta* **60**, 5101–5116.

Habermann G. M. (1978) Mineralogic and textural variations of the duricrust in southwestern Wisconsin. MS thesis, Univ. Wisconsin-Madison. p. 153.

Hervig R. L., Williams L. B., Kirkland I. K. and Longstaffe F. J. (1995) Oxygen isotope microanalyses of diagenetic quartz: possible low temperature occlusion of pores. *Geochim. Cosmochim. Acta* **59**, 2537–2543.

Heyl A. V., Agnew A. F., Behre, Jr., C. H., Lyons E. J. and Flint A. E. (1959) The geology of the upper Mississippi Valley zinc–lead district (Illinois–Iowa–Wisconsin). *U.S. Geol. Surv. Prof. Paper* 309, p. 310.

Hoholick J. D., Metarko T. and Potter P. E. (1984) Regional variations of porosity and cement: St. Peter and Mount Simon Sandstones in Illinois Basin. *Am. Assoc. Petrol. Geol. Bull.* **68**, 753–764.

Hu G. and Clayton R. N. (2003) Oxygen isotope salt effects at high pressure and high temperature and the calibration of oxygen isotope geothermometers. *Geochim. Cosmochim. Acta* **67**, 3227–3246.

IAEA (1981) Deuterium and oxygen-18 in the water cycle. In *Stable Isotope Hydrology* (eds. J. R. Gat and R. Gonfiantini). IAEA Tech. Rep. 210, p. 337.

Kelly J. L. (2006) Silcrete in the St. Peter Sandstone. MS thesis, Univ. Wisconsin-Madison, p. 124.

Khalaf F. I. (1988) Petrography and diagenesis of silcrete from Kuwait, Arabian Gulf. *J. Sed. Petrol.* **58**, 1014–1022.

Kita N. T., Ikeda Y., Togashi S., Liu Y., Morishita Y. and Weisberg M. K. (2004) Origin of ureilites inferred from a SIMS oxygen isotopic and trace element study of clasts in the Dar al Gani 319 polymict ureilite. *Geochim. Cosmochim. Acta* **68**, 4213–4235.

Kita N. T., Ushikubo T., Fu B., Spicuzza M. J. and Valley J. W. (2007) Analytical developments on oxygen three isotope analyses using a new generation ion microprobe IMS-1280. *Lunar Planet. Sci. XXXVIII*. #1981 (abstr.).

Labeyrie L. (1974) New approach to the surface seawater paleotemperatures using O^{16}/O^{18} ratios in silica of diatom frustrules. *Nature* **248**, 40–42.

Lee M. and Savin S. M. (1985) Isolation of diagenetic overgrowths on quartz sand grains for oxygen isotopic analysis. *Geochim. Cosmochim. Acta* **49**, 497–501.

Long J. D. (1988) Sedimentology of the Glenwood Member of the Middle Ordovician St. Peter Sandstone of southern Wisconsin. MS thesis, Univ. Wisconsin-Madison, p. 133.

Mackenzie F. T. and Gees R. (1971) Quartz: synthesis at Earth-surface conditions. *Science* **173**, 533–535.

Mai H. and Dott, Jr., R. H. (1985) A subsurface study of the St. Peter Sandstone in southern and eastern Wisconsin. *Wisc. Geol. Nat. Hist. Surv. Info. Circ.* 47, p. 26.

McBride E. F. (1989) Quartz cement in sandstones: a review. *Earth Sci. Rev.* **26**, 69–112.

McElhinny M. W. (1973). In *Paleomagnetism and Plate Tectonics*, (eds. W.B. Harland, S.O. Agrell, D. Davies and N.F. Hughes), p. 358. Cambridge Univ. Press, Cambridge.

McElhinny M. W. and Opdyke N. D. (1973) Remagnetization hypothesis discounted: a paleomagnetic study of the Trenton Limestone, New York State. *Geol. Soc. Am. Bull.* **84**, 3697–3708.

McLimans R. K. (1977) Geological, fluid inclusion, and stable isotope studies of the Upper Mississippi Valley zinc–lead district, Southwest Wisconsin. Ph.D. thesis, Penn. State Univ. p. 175.

Milliken K. L., Land L. S. and Loucks R. G. (1981) History of burial diagenesis determined from isotopic geochemistry, Frio Formation, Brazoria County, Texas. *Am. Assoc. Petrol. Geol. Bull.* **65**, 1397–1413.

Murray R. C. (1990) Diagenetic silica stratification in a paleosilcrete, North Texas. *J. Sed. Petrol.* **60**, 717–720.

Odom I. E., Willand T. N. and Lassin R. J. (1979) Paragenesis of diagenetic minerals in the St. Peter Sandstone (Ordovician), Wisconsin and Illinois. In *Aspects of Diagenesis* (eds. P. A. Scholle and P. R. Schluger). Soc. of Econ. Paleontol. Min. Spec. Publ. 26, pp. 425–443.

Ostrom M. E. (1967) Paleozoic stratigraphic nomenclature for Wisconsin. *Wisc. Geol. Nat. Hist. Surv. Info. Circ.* **8**, 4.

Paxton S. T., Szabo J. O., Ajdukiewicz J. M. and Klimentidis R. E. (2002) Construction of an intergranular volume compaction curve for evaluating and predicting compaction and porosity loss in rigid-grain sandstone reservoirs. *Am. Assoc. Petrol. Geol. Bull.* **86**, 2047–2067.

Pitman J. K. and Spotl C. (1996). Origin and timing of carbonate cements in the St. Peter Sandstone, Illinois Basin: evidence for a genetic link to Mississippi Valley-Type mineralization. In *Siliciclastic Diagenesis and Fluid Flow: Concepts and Applications* (eds. L. J. Crossey, R. Loucks, and M. W. Totten). SEPM Spec. Publ. 55, pp. 187–203.

Pitman J. K., Goldhaber M. B. and Spoetl C. (1997) Regional diagenetic patterns in the St.Peter Sandstone: implications for brine migration in the Illinois Basin. *U.S. Geol. Surv. Bull.*, 17–18.

Pittman E. (1972) Diagenesis of quartz in sandstones as revealed by scanning electron microscopy. *J. Sed. Petrol.* **42**, 507–519.

Prothero D. R. and Dott, Jr., R. H. (2004) *Evolution of the Earth*, seventh ed. McGraw-Hill, New York.

Rodas M., Luque F. J., Mas R. and Garzon M. G. (1994) Calcretes, palycretes, and silcretes in the Paleogene detrital sediments of the Duero and Tajo Basins, Central Spain. *Clay Mins.* **29**, 273–285.

Rowan E. L. and Goldhaber M. B. (1996) Fluid inclusions and biomarkers in the Upper Mississippi Valley zinc–lead district: implications for the fluid-flow and thermal history of the Illinois Basin. *U.S. Geol. Surv. Bull.* **2094-F**, 34.

Shepherd L. D., Drzewiecki P. A., Bahr J. M. and Simo J. A. (1994) Silica budget for a diagenetic seal. In *Basin Compartments and Seals* (ed. P. J. Ortoleva). Am. Assoc. Petrol. Geol. Spec. Publ. Mem. 61, pp. 369–384.

Sippel R. F. (1969) Sandstone petrology, evidence from luminescent petrography. *J. Sed. Petrol.* **38**, 530–554.

Sloss L. L. (1963) Sequences in the cratonic interior of North America. *Geol. Soc. Am. Bull.* **74**, 93–113.

Smale D. (1973) Silcretes and associated silica diagenesis in southern Africa and Australia. *J. Sed. Petrol.* **43**, 1077–1089.

Smith G. L., Dott, Jr., R. H. and Byers C. W. (1997) Authigenic silica fabrics associated with Cambro-Ordovician unconformities in the Upper Midwest. *Geosc. Wisc.* **16**, 25–36.

Spicuzza M. J., Valley J. W., Kohn M. J., Girard J. P. and Fouillac A. M. (1998) The rapid heating, defocused beam technique: a CO_2-laser based method for highly precise and accurate determination of $\delta^{18}O$ values of quartz. *Chem. Geol.* **144**, 195–203.

Sprunt E. S. and Nur A. (1981) Causes of quartz cathodoluminescence color. *Scan. Electron. Microsc.* **1**, 525–535.

Suchecki R. K. and Bloch S. (1988) Complex quartz overgrowths as revealed by microprobe cathodoluminescence. *Am. Assoc. Petrol. Geol. Bull.* 72, 252 (abstr.).

Sullivan M. D., Macaulay C. I., Fallick A. E. and Haszeldine R. S. (1997) Imported quartz cement in aeolian sandstone grew from water of uniform composition but has complex zonation. *Terra Nova* **9**, 237–241.

Summerfield M. A. (1983a) Petrography and diagenesis of silcrete from the Kalahari Basin, Cape Coastal Zone, southern Africa. *J. Sed. Petrol.* **53**, 895–909.

Summerfield M. A. (1983b) Silcrete as a paleoclimatic indicator: evidence from southern Africa. *Paleogeo., Paleoclimat., Paleoecol.* **41**, 65–79.

Sverjensky D. A. (1981) Isotopic alteration of carbonate host rocks as a function of water to rock ration – an example from the Upper Mississippi Valley zinc–lead district. *Econ. Geol.* **76**, 154–157.

Thiry M. and Millot G. (1987) Mineralogical forms of silica and their sequence of formation in silcretes. *J. Sed. Petrol.* **57**, 343–352.

Thiry M. and Milnes A. R. (1991) Pedogenic and groundwater silcretes at the Stuart Creek Opal Field, South Australia. *J. Sed. Petrol.* **61**, 111–127.

Thiry M. and Simon-Coincon R. (1996) Tertiary paleoweatherings and silcretes in the southern Paris Basin. *Catena* **26**, 1–26.

Valley J. W., Kitchen N., Kohn M. J., Niendorf C. R. and Spicuzza M. J. (1995) UWG-2, a garnet standard for oxygen isotope ratios: strategies for high precision and accuracy with laser heating. *Geochim. Cosmochim. Acta* **59**, 5223–5231.

Watts S. H. (1978) The nature and occurrence of silcrete in Tibooburra area of northwestern New South Wales. In *Silcrete in Australia*, (ed. H. Wopfner), pp. 167–193. University of New England, Australia.

Waugh B. (1970) Formation of quartz overgrowths in the Penrith Sandstone (Lower Permian) of northwest England as revealed by scanning electron microscopy. *Sedimentology* **14**, 309–320.

Webb J. A. and Golding S. D. (1998) Geochemical mass-balance and oxygen-isotope constraints on silcrete formation and its paleoclimatic implications in southern Australia. *J. Sed. Res.* **68**, 981–993.

Williams L. A. and Crerar D. A. (1985) Silica diagenesis, II. General mechanisms. *J. Sed. Petrol.* **55**, 312–321.

Winfree K. E. (1983) Depositional environments of the St. Peter Sandstone of the Upper Midwest. MS thesis, Univ. Wisconsin-Madison, p. 114.

Associate editor: Dimitri A. Sverjensky